Dynamical Climatology

A mass flux convection scheme with representation of cloud ensemble characteristics and stability dependent closure.

by

D. Gregory and P.R. Rowntree

DCTN 81

September 1989

Meteorological Office (Met. O. 20)
London Road
Bracknell
Berkshire RG12 2SZ

DYNAMICAL CLIMATOLOGY TECHNICAL NOTE NO. 81

A MASS FLUX CONVECTION SCHEME WITH REPRESENTATION OF CLOUD ENSEMBLE CHARACTERISTICS AND STABILITY DEPENDENT CLOSURE

by

D Gregory and P R Rowntree

Met O 20 (Dynamical
Climatology Branch)
Meteorological Office
London Road
Bracknell
Berkshire, UK RG12 2SZ

September 1989

NOTE: This paper has not been published. Permission to quote from it should be obtained from the Assistant Director of the above Meteorological Office branch.

ABSTRACT

The convection scheme used at the UK Meteorological Office in large-scale numerical models is described. The scheme uses a 'bulk' cloud model to represent an ensemble of convective clouds and aims to represent shallow, deep and mid-level convection. A simple closure is employed, the initial convective mass flux being related to the stability of the initial convecting layer. The ability of the scheme to represent convective processes in a variety of situations is evaluated using GATE and BOMEX and ATEX data. In each case realistic heating rates are simulated and although the closure of the scheme does not demand a balance between convective and large-scale forcings as in many other types of convection scheme (for example Kuo type and the Arakawa-Schubert schemes), a quasi-equilibrium is established while retaining realistic atmospheric structures.

The performance of the scheme in an 11-layer atmospheric general circulation model used in climate research at the UK Meteorological Office is also evaluated by comparing aspects of the simulated tropical flow from a recent four year integration with observed data. The scheme simulates the main areas of latent heat release and their variation throughout the year, although the Indian Monsoon is poorly simulated. The upper level divergent circulation is also well simulated although too weak in northern summer. The zonally averaged tropospheric temperature structure is reasonable indicating that the interaction of convective and radiative processes is reasonably modelled. The variation of outgoing longwave radiation (a proxy for convective rainfall in the tropics) with sea surface temperature agrees with recent observational studies.

1. INTRODUCTION

Cumulus convection plays an important role in the maintenance of the large-scale circulation of the atmosphere. However, when simulating such flow with numerical models, grid sizes are well above the scale of individual convective elements. Thus it becomes necessary to represent the net effect of an ensemble of convective clouds upon the atmosphere in terms of the grid scale parameters. Such a technique is referred to as cumulus parametrization

Cumulus parametrization (or convection) schemes have two goals. Firstly they must predict the net convective energy release in terms of known large-scale variables (the closure problem). Secondly in distributing this energy in the vertical a realistic thermodynamic structure must be maintained.

No full adequate theory exists for the closure problem. Observational studies suggest that deep convection is strongly related to the presence of low level convergence. This has formed the basis of several schemes (Kuo (1974), Anthes (1977)) in which convection rains out a proportion of the total moisture convergence (large-scale plus surface moisture flux) into a column of the atmosphere. Arakawa and Schubert (1974) developed a more complex theory in which an ensemble of convective elements are assumed to be in a quasi-steady state with the large-scale forcing. Recently Emanuel(1987) has critised the use of large-scale convergence as a criterion for the formation of convection. He points out that the growth

of convection requires only that the thermodynamic profile is conditionally unstable with respect to ascent, although if large-scale convergence or strong surface forcing is not present the profile will be quickly stabilised and convection will cease.

A theory for the vertical distribution of the convective heating/moistening is well established, being derived by several authors in the early 1970's (Ooyama (1971), Arakawa and Schubert (1974)) and recently being considered more fully using an explicit cloud model by Gregory and Miller (1989). Convection effects the large-scale atmosphere through subsidence in the cloud environment and detrainment of heat, moisture and liquid water from convective towers. However there is difficulty in defining such parameters, especially when it is necessary to consider an ensemble of convective clouds.

Observational studies have had some success in describing the effect of an ensemble of convective clouds on the large-scale flow using simple one-dimensional cloud models (Nitta (1978), Johnson (1980)). A number of convection schemes employ such cloud models and are termed mass flux schemes. Arakawa and Schubert's scheme considered a spectral ensemble of such models, each of differing characteristics to determine the vertical distribution of the convective heating/moistening. However because of the use of a spectrum of clouds the scheme is difficult to implement and although it has had some success has not received wide usage. However some observational studies have used simpler models of cloud ensembles with some success. Yanai et al (1973) successfully derived the convective heating for tropical waves over the Marshall Islands using a 'bulk' cloud model

i.e. one representing an average over all cloud types within a convective ensemble. Hence it may not be necessary to go to the complexity of using an ensemble of simple cloud models in convection schemes.

This paper describes a mass flux convection scheme utilising such a 'bulk' cloud model which is in use in large-scale atmospheric models at the UK Meteorological Office. The scheme aims to describe both dry and moist convection of all types (deep, mid-level and shallow). Although a single cloud model is used to represent the effects of an ensemble of clouds, account is taken of the clouds' varying characteristics and depths by allowing a proportion of the ensemble to undergo terminal detrainment before the maximum cloud height has been reached. Unlike most other convection schemes which assume a quasi-equilibrium state between convection and large-scale forcing to determine the amount of convective rainfall, the magnitude of convective activity is calculated by considering the stability of the lowest convecting layers only.

Results are presented from a study which has been recently initiated to consider the physical basis of the scheme and its performance in an 11-layer atmospheric general circulation model (AGCM) used in climate research at the UK Meteorological Office (described in Slingo and Pearson (1987) and Slingo et al (1989)), with a view to identifying ways in which the scheme's representation of convective processes could be improved. In the next section the scheme is described. Single column model tests of the scheme against a variety of observational data sets (GATE, BOMEX, ATEX) are presented in section 3. The performance of the scheme in the 11-layer climate model is considered in section 4, where multi-year seasonal mean

climatologies from a four year integration are compared with data obtained from the UK Meteorological Office archive of operational analyses and from other observational sources. Section 5 concludes with further discussion of the results and consideration of possible areas where the scheme might be improved.

2. THE CONVECTION SCHEME.

This is a penetrative convection scheme, applicable to both moist and shallow convection of all types (shallow, deep, mid-level). Lyne and Rowntree (1976) discussed the development of the scheme using GATE data while its use in a model of the tropical Atlantic (developed in conjunction with the GATE experiment) was briefly described by Rowntree and Cattle (1983). The scheme has undergone several modifications since being developed and various versions are used in large-scale atmospheric modelling at the UK Meteorological Office. The scheme described here is as used in the latest benchmark experiments of the 11-layer climate model used in climate research (Slingo et al (1989)). The 15-layer limited area forecast model uses an identical version while the 15-layer global forecast model uses an earlier version described briefly by Cunnington and Rowntree (1986) and more fully by Slingo (1985) (the main differences are in the treatment of precipitation processes and the detrainment of cloud air upon the termination of convection).

A single cloud model, based around parcel theory modified by entrainment and detrainment, is used to represent an ensemble of convective clouds, each of differing characteristics, terminating at different levels. Thus the parcel characteristics (temperature, mixing ratio, mass flux) calculated by the cloud model represent averages over the entire ensemble. For a column of the atmosphere, working from the bottom upward, each layer of the model is tested until one is found which, with a slight excess buoyancy s (0.2K, i.e that caused by a temperature excess of 0.2K), is

still buoyant by more than a lower limit b (set to 0.2K in the standard scheme) at the next layer after ascent, taking entrainment of environmental air into consideration. The convective process is then initiated. The parcel continues to rise, entraining environmental air and detraining cloudy air, until it is no longer buoyant after being lifted from layer k to the next model layer (k-1). It is then assumed that a proportion of the plumes represented by the parcel have reached zero buoyancy in layer k and have detrained there, the proportion being just sufficient to allow the parcel to be buoyant by 0.2K in layer k-1 . Hence allowance is made for the varying charcteristics of clouds within the assumed ensemble while still retaining a simple 'bulk' cloud model approach. This process (termed forced detrainment) allows buoyancy to increase indefinitely and so is restricted by two considerations which terminate the ascent of the parcel. Firstly a parcel cannot ascend higher than an undilute parcel from the starting layer of convection. Secondly, if the mass flux falls below a minimum value then the parcel is assumed to be destroyed by detrainment.

(a) Cloud model

The equations governing cloud mass flux (M), potential temperature (θ) mixing ratio (q) and cloud liquid water (l) as the parcel rises are

$$\frac{\delta M_p}{\delta \sigma} = (\varepsilon - \eta - \delta) M_p \qquad (1)$$

$$\frac{\delta \theta^p M_p}{\delta \sigma} = (\varepsilon \theta^E - \eta \theta^p - \delta \theta^R) M_p + \frac{LQ}{c_p} \qquad (2)$$

$$\frac{\partial q^P M_P}{\partial \sigma} = (\varepsilon q^E - \eta q^P - \delta q^R) M_P - Q \qquad (3)$$

$$\frac{\partial l^P M_P}{\partial \sigma} = -(\eta l^P + \delta l^R) M_P + Q - PR \qquad (4)$$

where M_P = cloud mass flux

ϕ^P = ϕ in cloudy air

ϕ^E = ϕ on environmental air

ϕ^R = ϕ on forced detrainment

ε = fractional entrainment rate

η = fractional mixing detrainment rate

δ = fractional forced detrainment rate

Q = conversion of water vapour to liquid water and ice

PR = liquid water and ice precipitated

L is the latent heat of condensation

and c_p is the specific heat of dry air

(Further explanation of the terminology is provided later.)

Figure 1 illustrates how these equations are discretised in the vertical for layer k (k decreasing upward). Environmental air is entrained at levels $k-\frac{1}{4}$ and $k-\frac{3}{4}$, while mixing and any forced detrainment occurs at level k. Condensational heating is added at level k-1. The discretised forms of equations (1), (2) and (3), after some manipulation, are

MASS

$$\begin{aligned} M_{k-1} = {} & M_k - \eta_k \Delta\sigma_{k-\frac{1}{2}} M_k - \delta_k (1-\eta_k \Delta\sigma_{k-\frac{1}{2}}) M_k \Delta\sigma_{k-\frac{1}{2}} \\ & + \varepsilon_{k-\frac{1}{4}} (1-\delta_k \Delta\sigma_{k-\frac{1}{2}}) (1-\eta_k \Delta\sigma_{k-\frac{1}{2}}) M_k \Delta\sigma_{k-\frac{1}{4}} \\ & + \varepsilon_{k-\frac{3}{4}} (1+\varepsilon_{k-\frac{1}{4}} \Delta\sigma_{k-\frac{1}{4}}) (1-\delta_k \Delta\sigma_{k-\frac{1}{2}}) (1-\eta_k \Delta\sigma_{k-\frac{1}{2}}) M_k \Delta\sigma_{k-\frac{3}{4}} \end{aligned} \qquad (5)$$

POTENTIAL TEMPERATURE

$$M_{k-1}\theta^{P}_{k-1} = M_k\theta^{P}_k - \eta_k\Delta\sigma_{k-1/2}M_k\theta^{P}_k - \delta_k(1-\eta_k\Delta\sigma_{k-1/2})M_k\theta^{R}_k\Delta\sigma_{k-1/2}$$
$$+ \varepsilon_{k-1/4}(1-\delta_k\Delta\sigma_{k-1/2})(1-\eta_k\Delta\sigma_{k-1/2})M_k\theta^{E}_k\Delta\sigma_{k-1/4} \qquad (6)$$
$$+ \varepsilon_{k-3/4}(1+\varepsilon_{k-1/4}\Delta\sigma_{k-1/4})(1-\delta_k\Delta\sigma_{k-1/2})(1-\eta_k\Delta\sigma_{k-1/2})M_k\theta^{E}_{k-1}\Delta\sigma_{k-3/4}$$
$$+ (L/c_p)COND_{k-1}$$

MOISTURE

$$M_{k-1}q^{P}_{k-1} = M_kq^{P}_k - \eta_k\Delta\sigma_{k-1/2}M_kq^{P}_k - \delta_k(1-\eta_k\Delta\sigma_{k-1/2})M_kq^{R}_k\Delta\sigma_{k-1/2}$$
$$+ \varepsilon_{k-1/4}(1-\delta_k\Delta\sigma_{k-1/2})(1-\eta_k\Delta\sigma_{k-1/2})M_kq^{E}_k\Delta\sigma_{k-1/4} \qquad (7)$$
$$+ \varepsilon_{k-3/4}(1+\varepsilon_{k-1/4}\Delta\sigma_{k-1/4})(1-\delta_k\Delta\sigma_{k-1/2})(1-\eta_k\Delta\sigma_{k-1/2})M_kq^{E}_{k-1}\Delta\sigma_{k-3/4}$$
$$-COND_{k-1}$$

CLOUD WATER

$$M_{k-1}l^{P}_{k-1} = M_kl^{P}_k - \eta_k\Delta\sigma_{k-1/2}M_kl^{P}_k - \delta_k\Delta\sigma_{k-1/2}(1-\eta_k\Delta\sigma_{k-1/2})M_kl^{P}_k \qquad (8)$$
$$+ COND_{k-1} - PREP_{k-1}$$

where φ_k is φ in layer k,

φ_{k-1} is φ in layer k-1,

φ^{R}_k is φ on forced detrainment in layer k,

φ^{P}_k is parcel φ in layer k

$COND_k$ is the water vapour sink due to condensation at level k

$= -M_k\gamma_k(q^{P}_k - q_s(\theta^{P}_k))$

$PREP_k$ is the amount of liquid water precipitated from the parcel at level k

$\Delta\sigma_{k-1/2} = \sigma_k - \sigma_{k-1}$,

$\Delta\sigma_{k-1/4} = \sigma_k - \sigma_{k-1/2}$,

$\Delta\sigma_{k-3/4} = \sigma_{k-1/2} - \sigma_{k-1}$

and γ_k =1 if parcel in layer K is saturated

=0 if unsaturated

An extra increment to the parcel temperature occurs when $(T^{E}_{K} + T^{E}_{K-1}) < 263K$ due to release of latent heat in freezing (263K is used as cloud water becomes super cooled before freezing occurs).

Several studies have been undertaken to determine the entrainment rate associated with convective plumes. Simpson and Wiggert (1969) and Simpson (1971) suggest a fractional entrainment rate which depend upon cloud radius R :

$$\varepsilon_z = 0.2/R$$

(for a height co-ordinate cloud model)

Transforming to sigma co-ordinates, $\varepsilon_\sigma = (p_*/\rho g)\varepsilon_z$. Assuming $p_* \simeq 1000mb$, $g \simeq 10ms^{-2}$ and $\rho \simeq 1$ $\varepsilon_\sigma \simeq 10^4 \varepsilon_z$. For shallow clouds with $R \simeq 500m$, $\varepsilon_\sigma \simeq 4$ while for deep clouds with $R \simeq 2000m$, $\varepsilon_\sigma \simeq 1$. Hence some variation of entrainment rate with height seems desirable. Near the surface both shallow and deep clouds will exist together, while if a plume reaches the upper troposphere only deep clouds remain. In the scheme the choice of

$$\varepsilon = 3A_E\sigma$$

is made. A_E (defined below) is usually set to 1.5 and so near the surface $\sigma \simeq 1$ and $\varepsilon \simeq 4.5$ reflecting the presence of both shallow and deep convection. At $\sigma \simeq 0.2$, $\varepsilon \simeq 1$ representing entrainment into deep convective towers. In the

discretised equations the two fractional entrainment rates are defined at $k-\frac{1}{4}$ and $k-\frac{3}{4}$ as

$$\varepsilon_{k-\frac{1}{4}}=3A_E\sigma_k$$

$$\varepsilon_{k-\frac{3}{4}}=3A_E\sigma_{k-\frac{1}{2}} \qquad (9)$$

where $A_E=1$ if $k=11$ (lowest layer)
and $A_E=1.5$ if $k<11$

Mixing detrainment of cloud air into the cloud environment is considered to occur in layer k at a rate of

$$\eta_k=(\varepsilon_{k-\frac{1}{4}}\Delta\sigma_{k-\frac{1}{4}}+\varepsilon_{k-\frac{3}{4}}\Delta\sigma_{k-\frac{3}{4}})(1-A_E^{-1})/\Delta\sigma_{k-\frac{1}{2}} \qquad (10)$$

The choice of A_E above implies that η_k is zero in the lowest model layer. Although Simpson (1971) defines $\eta\simeq\varepsilon$ no distinction is made in the scheme between turbulent entrainment and inflow into convective clouds. Hence detrainment is set less than entrainment to allow mass flux to increase with height. This is restricted by the process of forced detrainment which represents the outflow from those clouds in the ensemble which are no longer buoyant.

If on ascending from layer k to k-1, after entrainment, mixing detrainment and moist processes have been taken into account, the excess buoyancy of the parcel is less than a minimum value (b) ie.,

$$(\theta^P{}_v)_{k-1} - (\theta^E{}_v)_{k-1} < b$$

then forced detrainment is initiated in layer k. As described earlier, sufficient of the parcel is detrained (representing the terminal detrainment of its less buoyant members) to allow the parcel to be buoyant in layer k-1. The virtual potential temperature of the detraining air is set equal to that of layer k,

$$(\theta^R_v)_k = (\theta^E_v)_k \tag{11}$$

$$\text{ie. } \theta^R_k(1+0.61\gamma_k q_s(\theta^R_k)+0.61(1-\gamma_k)q^P_k) = \theta^E_k(1+0.61q^E_k)$$

$q_s(\theta^R_k)$ can be obtained from the Clausius-Clapeyron equation,

$$q_s(\theta^R_k) = q_s(\theta^E_k)(1+(L'/R_v(T^E_k)^2)(\theta^R_k-\theta^E_k)\sigma_k^x) \tag{12}$$

where L' = L when $(T^E_k+T^E_{k-1})>263K$

and = $(L+L_F)$ otherwise (L_F is the latent heat of fusion.)

However this leads to a quadratic in θ^R. Replacing $\theta^R_k q_s(\theta^R_k)$ by $\theta^E_k q_s(\theta^R_k)$ in the first term of equation (11) makes the equation linear in θ^R. This approximation incurs a fractional error in the moisture term of the virtual potential temperature of $(\theta^E_k-\theta^R_k)/\theta^R_k$. Using the alternative approximation of $q_s(\theta^R_k)\simeq q_s(\theta^E_k)$ incurs a larger error of $\simeq 20(\theta^E_k-\theta^R_k)/\theta^R_k$.

For a saturated parcel, solving for θ^R from equation (11) and (12),

$$\theta^R_k = \theta^E_k\left[\ 1 + \frac{0.61(q^E_k - q_s(\theta^E_k))}{1+0.61(L'/R_v T^E_k)q_s(\theta^E_k)}\ \right] \tag{13a}$$

For an unsaturated parcel equation (9) is linear in θ^R_K without approximation and on rearrangement,

$$\theta^R_K = \theta^E_K(1+0.61q^E_K)/(1+0.61q^P_K) \qquad (13b)$$

The parcel potential temperature in layer k-1 is obtained from the condition for buoyancy :

$$(\theta^P_v)_{K+1} = (\theta^E_v)_{K+1} + b$$

$$\text{ie. } \theta^P_{K-1}(1+0.61\gamma_{K-1}q_s(\theta^P_{K-1})+0.61(1-\gamma_{K-1})q^P_{K-1}) \qquad (14)$$

$$= \theta^E_{K-1}(1+0.61q^E_{K-1}) + b$$

in the same manner as that of equation (11).

For a parcel saturated in layer k-1,

$$\theta^P_{K-1} = \theta^E_{K-1}\left[\, 1 + \frac{0.61(q^E_{K-1} - q_s(\theta^E_{K-1})) + b}{1+0.61(L'/R_vT^E_{K-1})q_s(\theta^E_{K-1})} \,\right] \qquad (15a)$$

while for an unsaturated parcel,

$$\theta^P_{K-1} = (\theta^E_{K-1}(1+0.61q^E_{K-1}) + b)/(1+0.61q^P_{K-1}) \qquad (15b)$$

The detrainment rate δ_K is now obtained using equations (5), (6) and (7) together with values of θ^R_K and θ^P_{K-1} from equations (13) and (15).

The process of forced detrainment allows buoyancy to increase indefinitely and so it is necessary to limit it by two conditions by which the

convective process is terminated. Firstly, a parcel is not allowed to ascend higher than an undilute parcel from the starting level. Secondly, it is reasonable to assume that if the convective mass flux falls below a minimum value defined by,

$$M_{MIN}=10^{-3}cE_{MIN}$$

where E_{MIN} is 1K in the standard scheme,
and c is 3.33×10^{-4}

then the parcel is destroyed by entrainment. When convection terminates, the fraction $\delta_k\Delta\sigma_{k-\frac{1}{2}}$ of the parcel still detrains in layer k with neutral buoyancy, the remaining fraction $(1 - \delta_k\Delta\sigma_{k-\frac{1}{2}})$ detraining in layer k-1 with parcel values. (In the original scheme total detrainment of the parcel occurred in layer k with parcel values. This did not allow sufficient mixing between the boundary layer and the free atmosphere in regions of extensive shallow cumulus (e.g. the trade wind regions) producing too strong and too dry an inversion above a nearly saturated boundary layer. Slingo et al (1989) describes the impact of these changes upon the 11-layer model in detail).

(b) Impact on environment

As with all mass flux schemes the plume interacts with its environment through en/detrainment of heat, moisture and cloud liquid water and subsidence induced in the cloud environment which compensates for the parcel's upward mass flux (see Gregory and Miller (1989) for the theoretical derivation of the cumulus heating and moistening rates due to

these processes). Considering fluxes of θ, q and l between cloud and environment in layer k and vertically out of and into layer k (fig 1), the net change in a time Δt of the environmental potential temperature, θ^E_K, and specific humidity, q^E_K, are given by,

$$\Delta\theta^E_K = (M_K \Delta t/\Delta\sigma_K)\{ (1+\varepsilon_{K-\frac{1}{4}}\Delta\sigma_{K-\frac{1}{4}})(1-\delta_K\Delta\sigma_{K-\frac{1}{2}})(1-\eta_K\Delta\sigma_{K-\frac{1}{2}})(\theta^E_{K-1}-\theta^E_K)$$

$$+ \delta_K\Delta\sigma_{K-\frac{1}{2}}(1-\eta_K\Delta\sigma_{K-\frac{1}{2}})(\theta^R_K-\theta^E_K) + \eta_K\Delta\sigma_{K-\frac{1}{2}}(\theta^P_K-\theta^E_K) \qquad (16a)$$

$$- (L'/c_p)(\eta_K\Delta\sigma_{K-\frac{1}{2}} + \delta_K\Delta\sigma_{K-\frac{1}{2}}(1-\eta_K\Delta\sigma_{K-\frac{1}{2}}))l^P_K \}$$

$$\Delta q^E_K = (M_K \Delta t/\Delta\sigma_K)\{ (1+\varepsilon_{K-\frac{1}{4}}\Delta\sigma_{K-\frac{1}{4}})(1-\delta_K\Delta\sigma_{K-\frac{1}{2}})(1-\eta_K\Delta\sigma_{K-\frac{1}{2}})(q^E_{K-1}-q^E_K)$$

$$+ \delta_K\Delta\sigma_{K-\frac{1}{2}}(1-\eta_K\Delta\sigma_{K-\frac{1}{2}})(q^R_K-q^E_K) + \eta_K\Delta\sigma_{K-\frac{1}{2}}(q^P_K-q^E_K) \qquad (16b)$$

$$+ (\eta_K\Delta\sigma_{K-\frac{1}{2}} + \delta_K\Delta\sigma_{K-\frac{1}{2}}(1-\eta_K\Delta\sigma_{K-\frac{1}{2}}))l^P_K \}$$

The first term in these expressions represents compensating subsidence, the second and third forced and mixing detrainment respectively. The last term is the effect of the detrainment of cloud condensate. Changes of phase and evaporation of precipitation also contribute to the environmental temperature and moisture changes and are considered in the following section.

(c) Precipitation processes.

The development of precipitation in shower clouds occurs mainly by the coalescence of smaller drops of water with larger ones. As discussed by Ludlam (1980, chapter 8) the rate at which this occurs depends upon the

distribution of the aerosol size spectrum, so that clouds which form in air masses with greater numbers of large nuclei (r>20μm) present precipitate earlier. This is reflected in the differing depths that clouds have to attain in maritime and continental air masses for precipitation to be initiated. This depth is greater for nucleus-rich continental air (3 to 5 km) than for maritime air (1 to 2 km) which has fewer but typically larger condensation nuclei (table 8.3 in Ludlam (1980, chapter 8)). Although the glaciation of a cloud is not necessary for the formation of precipitation, clouds whose tops exceed the -10°C level by 1 km will produce precipitation by the growth of hail from the freezing of super cooled water droplets.

The aerosol distribution of air is not available in the model but these observations are reflected in the convection scheme by suppressing the precipitation of condensed water until the cloud has exceeded a critical depth, D_{CRIT} (base to top) and the amount of cloud condensate within the parcel (l^P_k) exceeds a minimum value l_{MIN}. Until these criteria are met no precipitation occurs and the condensed water is stored within the parcel as the ascent continues. In the standard scheme l_{MIN} is set to 1g/kg or the local saturation specific humidity where it is less, while D_{CRIT} is defined by,

$$D_{CRIT} = \begin{cases} 4.0\text{km over land} \\ 1.5\text{km over sea} \\ 1.0\text{km if } T_{k-1} < 263\text{K} \end{cases}$$

These crudely take into account variations of atmospheric aerosol over land and sea and also the observation that precipitation forms in clouds soon after glaciation.

If these criteria are met, the amount of precipitation produced in g/cm²/s, over a time step, in taking the ensemble from level k to k-1 is,

$$P_K=(1^P{}_{K-1}-l_{MIN})M_{K-1}(10p_*/g) \qquad (g/cm^2/s) \quad (17)$$

Here p_* is in mb and g in ms^{-1}. l_{MIN} of the condensate is retained by the parcel in the process. Total precipitation falling from cloud base is obtained by summing P_K between cloud base and cloud top.

Freezing and melting of falling precipitation occurs at the freezing level of the environment and the model temperature fields are changed accordingly. Falling snow is not evaporated but falling rain is allowed to evaporate below cloud base; the rate is proportional to the sub-saturation of the environment and is constructed by integrating the fractional evaporation of precipitation over a layer of depth dz ie,

$$dJ/J=\beta(q-q_s)\rho dz/Q \qquad (18)$$

where ρ is the density of air, Q is the local rainfall rate estimated by assuming precipitation covers 10% of a grid box ($Q=10J_B$ where J_B is the grid box mean rainfall at cloud base) and β is a constant set to $10^{-3}s^{-1}$ in the standard scheme (based upon Kessler (1969)).

If the air is not saturated the precipitated water J_K reaching level k from level k-1 is given by,

$$J_K=J_{K-1}\exp[-\beta p_*\Delta\sigma_K[q_s(T^E{}_K)-q^E{}_K]/[J_B g]] \qquad (g/cm^2/s) \quad (19)$$

where J_k is in g/cm²/s, p_* in mb and q in Kg/Kg.

Mixing ratio and temperature increments due to evaporation are

$$\Delta q_k = (J_{k-1} - J_k)g\Delta t/(10p_*\Delta\sigma_k)$$

$$\Delta T_k = -(L/c_p)\Delta q_k$$

(d) Closure

To complete the scheme the overall magnitude of the convective energy release must be determined in terms of known large-scale variables (the closure problem). For mass flux schemes this is achieved by specifying the mass flux in the layer from which the plume began its ascent. Most convection schemes achieve this by assuming a quasi-equilibrium between convection and large-scale forcing processes as in Kuo type and Arakawa-Schubert schemes. Here a different approach is used. The mass flux of the plume in the initial convective layer (M_I) is simply related to the stability of the lowest convecting layers by the empirical formula;

$$M_I = 10^{-3}c[\{(\theta^P{}_v)_{k-1} - (\theta^E{}_v)_{k-1}) - b\}/\Delta\sigma_{k-\frac{1}{2}}] \quad (s^{-1}) \qquad (20)$$

where c is 3.33×10^{-4}

ie the initial mass flux is proportional to the excess buoyancy of the parcel in layer k-1, the parcel starting from layer k.

With such a formulation convection can occur without the presence of large-scale convergence, although it would quickly cease without the convergence compensating the warming and drying due to convection above the boundary layer. The constant 'c' determines the convective mass flux per unit increase in parcel buoyancy with height across the initial convecting layer. Hence the larger the value of 'c' the more convective mass flux is generated for a given atmospheric stability. The value of 'c' was chosen to give a realistic atmospheric thermodynamic structure and surface rainfall rate and also to ensure that there was not an excessive growth in conditional instability within a column of the atmosphere, which might lead to the risk of computational instability .

(e) Energy conservation

Once all the increments have been calculated a check is made to ensure enthalpy is conserved,

$$c_p \int_1^0 \Delta T d\sigma + L \int_1^0 \Delta q d\sigma = L_F \int_1^0 \Delta_s q_F d\sigma \qquad (21)$$

where L_F is the latent heat of fusion,
q_F is the ice content,
and Δ_s is the increment due to changes in phase only.

This integral is satisfied by reducing those temperature increments which are of the same sign as the residual. The imbalance arises due to inaccuracy in calculating the temperature along a moist adiabat and also the discretisation of the cloud model in the vertical.

3. SINGLE COLUMN MODEL EXPERIMENTS

The performance of the convection scheme is first discussed using a single column model. The ability of the scheme to represent deep convection is studied using GATE data, while for studies of shallow convection BOMEX and ATEX data are employed. These three data sets were chosen, firstly because there are few good observational data sets available and secondly because they have been employed in recent years to test a variety of convection schemes (Betts and Miller (1986) and Tiedtke (1988)). Hence comparison may be made between various schemes, although results will also depend upon the details of the model used.

(a) The single column model

The single column model is based upon the 11-layer atmospheric general circulation model (AGCM) employed in climate research at the UK Meteorological Office. A time step of 15 minutes is used. Sigma co-ordinates are used in the vertical with model levels at sigma = 0.98744, 0.93701, 0.84380, 0.71772, 0.57717, 0.43626, 0.31738, 0.23047, 0.15741, 0.08856 and 0.02207. A variety of physics schemes are available as described in Slingo (1985). In these experiments they are:-

(1) Radiation - radiative fluxes are specified using the temperature and moisture profiles and cloud amounts (high, medium, low, and convective); the cloud amounts and levels

are derived from the large-scale precipitation and convection schemes. Cloud radiative properties are prescribed.

(2) Boundary layer - Clarke formulation (Clarke(1970), Carson(1982a)). Surface fluxes are mixed upward in stable and neutral conditions only - convective mixing is assumed to be sufficient in unstable conditions. The boundary layer exists in the lowest three model layers.

(3) Large-scale precipitation - occurs when supersaturation exists. The ice phase is considered and both snow and rain are evaporated as they fall, the rate depending upon the sub-saturation of the atmosphere and a rate constant β set to $2\times10^{-5}s^{-1}$.

(4) Convection scheme - the mass flux scheme previously described

(b) GATE data

Data from the composite GATE easterly wave data set of Thompson, Payne, Recker and Reed (1979) (henceforth referred to as TPRR) were employed to test the ability of the scheme to represent deep convection. The data set represents an easterly wave of approximately 80 hours duration. Eight wave categories are defined, category 8 being when the ridge of the wave is over the GATE area, category 4 the trough. The model thermodynamic and wind profiles are initiated with data from the centre of category one (referred to as 0 hours of the simulation). Averages over ten hour periods are used in the presentation of results the first being centred on 5 hours into the

simulation. They are thus 5 hours out of phase with the categories defined by TPRR. Figure 2 presents a T-Φ gram of the initial profiles. Surface pressure is taken as 1013mb and air lifted from the lowest model level (≃1000mb) reaches saturation at 955mb and the level of free convection at 950mb. With undilute ascent cloud top zero buoyancy is reached at 150mb, indicating that deep convection is possible once initiated.

Profiles of heating and moistening by large-scale processes were obtained from TPRR and presented to the model (fig 3 - averages over the wave cycle). Radiative heating rates were calculated by the radiation scheme (fig 3 - average over wave cycles 2 through 6). Horizontal and vertical advection produce a cooling maximum around 600mb and moistening which peaks near 850mb. Radiative cooling over the wave cycle peaks in the boundary layer of the model and gradually decreases with height. TPRR used a profile attributable to Dopplick (1972) in their diagnosis of diabatic heating/moistening. In the lower troposphere this has a similar structure in the vertical but also exhibits a peak in cooling between 400 and 500mb of ≃-2K/day. Surface fluxes are not calculated using the boundary layer scheme but are specified from observations. These are allowed to vary linearly from the values observed as the temperature difference between the lowest model layer and the sea surface (fixed at 27°C) departs from reality as the simulation proceeds.

The model was integrated forward for 20 days (6 wave cycles, the evolution of large-scale forcing repeating every 80 hours). Results presented are composited over wave cycles 2 through 6. Wave cycle 1 (the first 80 hours

of the experiment) is excluded because of the spin-up of the model during the first 10 - 20 hours of the simulation. During this period the convection is out of balance with the applied forcing.

The evolution of rainfall over the wave is reasonably represented by the scheme (fig 4 - average over 10 hour periods) although the peak magnitude is approximately 60Wm^{-2} less than observed. Some of this discrepancy is caused by the modelled surface evaporation being less than observed over the wave (86Wm^{-2} c.f. 106Wm^{-2}) due to the lowest model layer being wetter than observed. (Sensible heat flux is larger than observed, 28Wm^{-2} c.f. 10Wm^{-2} due to the lowest model layer being cooler than observed).

The evolution of rainfall is similar in shape to the moisture forcing prescribed to the model, although changes in rainfall lag those of moisture forcing by around 10 hours. Between 70 - 80 hours and 0 - 20 hours the modelled rainfall rate is smaller than the moisture forcing. This storage of moisture is a feature of the observations. The convection scheme does not model it fully, rainfall increasing more rapidly between 70 and 80 hours than observed. In the real atmosphere storage is caused by the drier air of the ridge suppressing convection through entrainment processes in growing plumes. In the case of the convection scheme the control of convective activity takes place mainly in the lowest two model layers from which the convective mass flux is determined (demonstrated later). The boundary layer becomes excessively stable during the simulation due to the evaporation of convective rainfall below cloud base only, in this instance the lowest model layer. This inhibits convection in the first half of the wave cycle, convection increasing as the boundary layer warms and moistens

from the ridge to the trough (by 0.3K and 0.2g/Kg). It should be noted that this disagrees with the observed evolution of the lowest model layer mixing ratio which decreases from 17.4g/Kg in the vicinity of the ridge to 17.0g/Kg as the trough crosses the GATE area.

The evolution of Q1 and Q2 (convective, boundary layer and dynamical rain heating and moistening respectively) are reasonable (fig 5) when compared with the observed distribution. Q1 peaks around 600mb but there is too little heating above 500mb This may be due to the differences in radiative heating profile calculated by the model and that used by TPRR in their diagnosis of Q1. Dopplick's profile shows a greater cooling above 500mb which would increase the convective heating diagnosed in this region. The structure and magnitude of Q2 is also reasonable, peaking between 800 and 900mb.

Q1 and Q2 generally follow the evolution of the prescribed large-scale cooling and moistening (not shown), although important departures occur as discussed when the evolution of surface rainfall was considered (fig 4), the response of convection being modulated by the thermodynamic structure. However in the easterly wave data set of TPRR no change in thermodynamic structure occurs over the entire wave cycle, the convection being in equilibrium with the forcing. The convection scheme models this well over the entire wave cycle, convection and the prescribed forcing being in equilibrium to within a few percent. Generally for the tropical convective atmosphere only small changes (<1K) are seen in the temperature structure over several days (Lord and Arakawa (1980)). Thus convection balances the forcing and keeps the temperature structure reasonably constant. Hence a

convection scheme must not only be able to reproduce the vertical structure of the observed convective heat source but must also retain a reasonable thermodynamic structure as it does so.

Figure 6 shows the mean thermodynamic profile over the entire wave cycle compared to that observed. The structure is generally retained. Much of the troposphere is warmer than observed although the lowest model layer is cooled due to the evaporation of rain. In general the simulation of the moisture structure of the atmosphere by convection schemes is worse than for temperature. With the present convection scheme the lower troposphere is too dry (except for the lowest model layer which is wetter than observed due to the evaporation of rain below cloud base) while above 700mb the atmosphere is too wet. Such a feature seems common to a wide variety of convection schemes being evident, in both the mass flux scheme of Tiedtke (1988) and the adjustment scheme of Betts and Miller (1986) when using the same GATE data.

Much of this change in thermodynamic structure occurs in the first wave cycle and is related to the spin-up of the model. Figure 7 compares the deviations of the average temperature and moisture profiles for wave cycle 1 and 2 through 6 from those observed. Little structural difference is seen, implying there is little drift over the integration apart from that occurring during the first wave cycle. (The large temperature drift above 200mb occurs above the top of the convective layer and is caused by the applied forcing not being balanced by convective processes). Initially the convective heat release is too large, greater than the cooling due to large-scale forcing and radiation. The thermodynamic structure adjusts

allowing the convection scheme to come into a quasi-equilibrium with the forcing processes. Over the entire wave cycle equilibrium is achieved to better than 1%, the average latent heat forcing for wave cycles 2 through 6 being 348Wm^{-2} while the surface rainfall is 350Wm^{-2}. It is important to note that this equilibrium is not constrained explicitly by the closure hypothesis of the scheme which only specifies the 'efficiency' of convection in terms of atmospheric stability. Balance is achieved purely through the adjustment of the thermodynamic profile under the action of convection and other forcing processes.

This is further illustrated by figure 8 which shows the convective heating response to the observed and modelled mean soundings over the wave cycle (both presented in figure 6) obtained by integrating the single column model forward for one time step (with these profiles used as the initial conditions). With the observed sounding the convective heating is out of balance with the temperature forcing throughout the cloud layer whereas the balance is naturally good with the modelled sounding.

Several experiments were carried out with hybrids of the two profiles to determine the role played by various parts of the thermodynamic structure in achieving the quasi-equilibrium between convection and the supplied forcing. Using the modelled temperature structure in the two lowest model layers with the observed temperature and moisture structure elsewhere, the profile is too stable for convection to occur. Introducing the modelled moisture structure as well into layers 11 and 10 allows convection to occur, the heating exceeding the cooling due to the supplied forcing below 700mb by between 1 and 2K/day, but having the structure above this of the

convective heating with the pure observed profile. The surface rainfall is also similar to that with the observed profile, 381Wm^{-2} compared with 396Wm^{-2}. Using the modelled temperature for layer 9 to layer 4 (but not below layer 9) brings the convective heating into balance with the temperature forcing above 600mb, but remains out of balance below this (by around 3K/day). The rainfall is reduced by 10% from that for the observed profile case.

These results indicate that the thermodynamic structure in the lowest two model layers (from where the convective mass flux is determined in this case) play a dominant role in determining the response of the convection scheme to forcing processes. The temperature structure above this evolves so as to bring the convective heating into balance with the forcing processes above 600mb. However their effect upon the net latent heat release is small as the moisture content of the atmosphere is much reduced at these upper level compared with the lower troposphere.

Several experiments were carried out to test the sensitivity of the scheme to changes in internal parameters. Little impact upon the diabatic heating distribution in the vertical or with time was seen, each experiment coming into equilibrium with the applied forcing. However different temperature structures evolved during the spin-up to achieve this (fig 9 - averages over wave cycles 2 through 6). Increasing the amount of liquid water retained by the parcel to 2g/kg (from 1g/kg) has little impact, the temperature profile being slightly cooler than with the standard scheme in the lower troposphere. The mid-troposphere is also wetter (by 0.5g/kg) due to greater amounts of cloud water being detrained. Doubling entrainment

rates and reducing the parameter 'c' used in determining the initial mass flux by an order of magnitude (to 3.33×10^{-5}) each give still cooler atmospheres. Increased entrainment implies a weaker parcel ascent and so more forced detrainment leading to reduced subsidence and consequent cooling of the atmosphere under the action of the unbalanced large-scale forcing and radiation. This reduces forced detrainment, so allowing the convection to come into balance with the forcing. Similarly with a reduction of the initial mass flux parameter, cooling leads to less forced detrainment, hence allowing the parcel mass flux to increase more rapidly with height. This is aided by the lowest two model layers being less stable than in the other simulations (by $\simeq$0.75K) therefore increasing the buoyancy of air in layer 10 on ascent from layer 11, which, with 'c', controls the initial mass flux (see eqn (20)).

These experiments illustrate an important point concerning convection schemes. The net latent heat release in each experiment is similar, showing that the scheme is able to come into equilibrium with the applied forcing in terms of detailed vertical structure as well as for the total energy budget. However the thermodynamic structure evolves to achieve this according to the 'constraints' within the scheme. This quasi-equilibrium thermodynamic structure must represent the observed atmospheric structure well if the scheme is to provide a reasonable representation of convection. In the experiments presented, although the equilibrium profiles differ from those observed, in the convective layer deviations from the observed temperature structure are mostly less than 2K. Hence the scheme appears robust to reasonable changes to its internal parameters.

(c) BOMEX data

Data derived from Holland and Rasmusson (1973) were used to initialise the model (fig 10). These data represents the average thermodynamic profile over a five day period (between June 22nd and 26th 1969). The inversion seen by the model is weaker than that observed due to the positioning of model levels in the vertical. Advective forcing is supplied to the model from the observations and is kept constant throughout the simulation. Radiative and surface forcing is supplied by the model physics. Sea surface temperature is fixed at 29°C throughout and the surface pressure at 1013mb. A one day experiment was carried out, results presented being averaged between 6 and 24 hours.

During the first six hours of the simulation deep convection occurs due to the weakness of the inversion as seen by the model. Increasing the temperature in layer 8 of the model (≃730mb) suppresses deep convection throughout the experiment but the necessary change was felt to be too large. After 6 hours, only shallow convection is present, being limited to the lowest four model layers. Fig 11 illustrates the transport properties of the shallow convection between 6 and 24 hours, no net surface rainfall being produced. Convection transports heat and moisture supplied by the boundary layer upwards into the inversion, the consequent cooling (caused by the evaporation of detrained liquid water) and moistening balancing the net warming and drying due to subsidence less radiation. The cooling by convection in the inversion layer is mainly caused by the detrainment of air cooler than the environment from clouds, the evaporation of detrained cloud liquid water accounting for only 10 - 20% of the cooling. The total

diabatic forcing of sensible heat is in good agreement with the observations (Fig 12) the boundary layer being warmed while the inversion layer is cooled.

Profiles of T and q over the same period are in reasonable agreement with the observations (fig 10). Generally the atmosphere is warmed slightly below the inversion and the inversion strengthened slightly (T_s-T_s increasing by 0.2K). The boundary layer dries out and moistening occurs above the inversion. However approximately 50% of these changes take place during the first six hours of the simulation when deep convection occurs and would seem to be a consequence of the convection and forcing being out of balance during this period.

Several experiments were carried out to test the sensitivity of the scheme to variations in the magnitude of the initial mass flux and the entrainment rates. Halving the initial mass flux parameter 'c' reduces the intensity of the convection but does not eliminate the deep convection altogether. Although deep convection dies out after the first six hours of the simulation it recurs during the last three hours. Doubling the entrainment rates also produces a weaker plume but again does not eliminate the initial deep convection. Although both experiments produce different temperature profiles averaged over the last 18 hours of the simulation neither can be said to be a real improvement on that of the standard scheme.

(d) ATEX data

ATEX data (Augstein et al (1973)) were also used to test the ability of the scheme to represent shallow convection. The model was initialised with thermodynamic and wind profiles representing averages over the ATEX undisturbed period (7 - 12 February 1969) (fig 13). The inversion is stronger than for the BOMEX case and the problem of the occurrence of deep convection near the start of the simulation was not encountered. Forcing data were prescribed as in previous experiments. The surface fluxes over this period of ATEX were $14Wm^{-2}$ and $208Wm^{-2}$ for sensible and latent heat respectively (Krügermeyer (1976)).

The model was integrated forward for one day. Convective transports of heat and moisture averaged over this period (fig 14) were similar to those for BOMEX, convection cooling and moistening the inversion layer in opposition to the warming and drying by subsidence. Too much moisture is transported above the inversion (fig 13 - $\simeq$700mb). This is not balanced by drying due to subsidence. A similar feature appears in the BOMEX simulation (fig 10) suggesting that the upward transport of moisture across the inversion by shallow convection is overestimated by the process of split final detrainment (described in section 2(a)). The strength of the inversion is reasonably well retained being weaker than observed by 0.5K. Below the inversion the atmosphere is warmed and dried (except in the lowest model layer).

Experiments varying several parameters of the scheme (similar to those using BOMEX data) were carried out. However the general thermodynamic

structure was unchanged. Doubling entrainment rates has some impact upon the moisture structure above the inversion, the mixing ratio in layer 8 (≃730mb) being reduced by ≃0.5g/kg (around 50% of the deviation from observations seen with the standard scheme), due to weaker plumes penetrating less into the inversion layer.

4. PERFORMANCE IN AN 11-LAYER ATMOSPHERIC GENERAL CIRCULATION MODEL.

Convection plays an important role in maintaining the atmospheric circulation. This is especially so in the tropics. Hence validation of the tropical circulation in an atmospheric general circulation model against observed data provides some indication of the performance of a convection scheme. In this section the tropical circulation of a recent integration of the UK Meteorological Office 11-layer climate model is briefly described. This is a finite difference model with a 2.5 by 3.75 degree latitude-longitude grid described by Slingo and Pearson (1987) and Slingo et al (1989). The physics of the model is identical to that of the single column model described in the previous section, except that in the boundary layer scheme the mixing coefficients are dependent upon the stability of the atmosphere (Richards (1980)).

Slingo et al (1989) present results from a four year integration of the model, concentrating upon the prediction of cloudiness and the earth's radiation budget. Consideration was given to the convection scheme's representation of shallow convection and it was noted that split final detrainment (section 2a) overestimated the transport of moisture above the inversion, weakening the hydrolapse compared to the observed data (fig 6 of Slingo et al (1989)) in a similar manner to that found in the BOMEX and ATEX experiments described previously. However little consideration was given to the representation of deep convection apart from convective cloud amounts and outgoing longwave radiation.

Figure 15 compares the surface rainfall distribution for northern winter (Dec, Jan, Feb) (DJF) and summer (Jun, Jul, Aug) (JJA) averaged over the four year integration of Slingo et al (1989) with the observed climatology of Jaeger (1976). Most of the main precipitation features during both seasons are simulated, but there are substantial differences between the modelled intensities and those estimated by Jaeger. To some extent this is no doubt due to the uncertainties in the observed estimates. For example, the east Pacific convergence zone near 5°N is stronger in the model in both seasons. However, the estimate by Jaeger is well below those by Taylor (1973), and Dorman and Bourke (1979), who both estimate peak values exceeding 10 mm/day throughout the east Pacific from about 180° to the South American coast in JJA; this also holds for Taylor's estimate in DJF, though Dorman and Bourke then show over 10 mm/day only from about 130-170°W. Taylor's estimates are based on data from low-lying islands and satellite cloud analyses, while Dorman and Bourke used ship rainfall frequencies and subjective intensities. Jaeger's analysis and also that of Reed and Elliott (1979) were derived in a similar manner to Dorman and Bourke's, but different conversions between subjective and quantitative intensities were employed. Kilonsky and Ramage (1976) obtained values less than Taylor's but, at 8 to 9 mm/day for the annual mean, zonal mean near 5°N, they were in reasonable agreement with the model; they used a regression relation between rainfall measured on atolls and satellite visible reflectivities.

In the dry zones of the eastern tropical oceans, the regions with less than 0.1 mm/day in the model appear to be too dry. There are also deficiencies in model rainfall near the equator in the west Pacific and Indian Oceans;

minima are evident in the cloud cover analyses by Miller and Feddes (1971) for these regions, but estimates of rainfall data do not support the intensity of these modelled minima. During DJF, the ITCZ is too weak over the Atlantic and west Africa (to the south of the equator). The precipitation maximum over South America is well simulated although rainfall over Indonesia (the other main area of latent heat release in the tropics during this season) is less satisfactory. In this region too much precipitation is simulated north of the equator, while the South Pacific Convergence Zone is too weak south of about 25°S. Rainfall is too heavy over northern Australia.

During JJA, the northward shift of the tropical precipitation belts is captured, the main regions of heat release in the observed climatology being over Central America, India and southeast Asia, and the west Pacific. Rainfall over Central America is overestimated while northern Brazil is too dry. The rain belt over Africa is also under estimated although well located. A major error in the simulation is the lack of monsoon rainfall over the Indian sub-continent.

Regions of intense precipitation are associated with ascent and upper level divergence. Figure 16 shows the velocity potential (the Laplacian of which is the divergence) and divergent wind field at 200mb for northern winter and summer, together with difference maps from seasonal means of the Meteorological Office archive of operational analyses meaned over the years 1982 to 1985. The main centres of upper level divergence are simulated reasonably well. During northern winter the model overestimates the divergence over South America and East Africa (south of the equator). This

is associated with excessive upper level convergence over the equatorial Atlantic, which is linked to the underestimation of rainfall in the Atlantic ITCZ. The divergent flow over Indonesia is too weak, leading to a weakening of the Hadley and Walker circulations over the tropical Pacific. During the northern summer the lack of monsoon rainfall over India is associated with weakening of the strong upper tropospheric divergence over this region.

The main features of the low level flow are also captured by the model (Fig 17). During northern summer the Indian Monsoon jet is well placed although maximum winds are too low. The jet also extends slightly too far out over the west Pacific. The winds to the west of central America are reversed in the model while the maximum in easterly winds over the tropical Atlantic is misplaced to the east. These errors in the simulated circulation are associated with the excessive latent heat release over Central America at this time. During northern winter the main circulation features are present although over the tropics and sub-tropics easterly winds are overestimated, especially in the Pacific and western Atlantic.

This comparison of the model and observed fields shows that the tropical simulation is reasonably satisfactory with the major exception of the summer monsoon rains over India. However many factors play a role in the development of the monsoon (orography, land surface processes, radiation, model resolution) and so failure to capture this part of the flow does not necessarily indicate a failure of the convection scheme. Thus, with this proviso, the convection scheme seems to be able to simulate the magnitude and distribution of the main tropical heat sources.

Over the oceans, further evidence on the realism of the tropical rainfall distribution can be obtained from a study of the variation of outgoing longwave radiation (OLR) at the top of the atmosphere against sea surface temperature (SST) for convective regions. Figure 18 presents a plot of OLR against SST for the simulation (calculated for grid points warmer than 22°C, averaged over four years and all seasons) together with results from an observational study (Graham and Barnett (1987)). In both cases OLR has been averaged over 0.5°C bins of SST. The observations suggest that deep convection does not occur until the SST is greater than 27°C, indicated by the rapid decrease in OLR above this and so colder cloud top temperatures. The modelled OLR shows little sensitivity to SST below 27°C but a rapid decrease above this (in a similar manner to the observations). Hence the response of model cloud in regions of deep convection to increasing SST compares favourably with observation, suggesting that the distribution of tropical precipitation simulated by the model is reasonable. However, minimum values of OLR in convective regions are upto 20 Wm^{-2} lower than observed and this is discussed further below.

Slingo et al (1989) noted that the model values of OLR were too low in the tropics. This emission is not directly from convective cloud tops but from more extensive layer cloud associated with the outflow of moist air from deep convective cloud. The low simulated values of OLR in these regions may be due to any of a number of factors; the cloud tops may be too cold or cloud amounts too large. A further possibility is that high cloud emissivity, set at 0.67, is too large for tropical cirrus. However the converse is likely to be the case, the thick tropical cirrus associated with deep convection being observed to have emissivities approaching unity.

Cloud tops may be too cold through being placed too high in the model or through the model being too cold in the upper troposphere. In the tropics the convection scheme predicts cloud tops between 400 and 200mb (Fig 11 of Slingo et al (1989)). It is difficult to verify the first hypothesis because of the lack of direct data concerning cloud top heights. However comparison of the zonal average temperature in the tropics and sub-tropics with observations (Fig 19) suggests that the model is too cold by 1-2K around 300mb during both summer and winter, consistent with the lower values of OLR seen in fig 18. However the temperature error can only account for at most 10 Wm^{-2} of the difference between the modelled and observed OLR in convective regions. This suggests that the model overestimates the amount of high cloud in the tropics. It is consistent with this that C. Wilson (personal communication), experimenting with the UK Meteorological Office global forecast model and using physics similar to those being discussed here, notes a similar temperature error in the upper tropical troposphere which is found to be associated with excessive cloud amounts.

It should be noted that the tropical tropospheric temperature errors in figure 19 are less than those found in some other climate models. Schlesinger and Mitchell (1985) compare zonal temperature errors for the GISS, NCAR and GFDL climate models. The GISS model shows a warming of 5K above climatology during both northern summer and winter in the upper troposphere. The NCAR model has temperatures 10K too low near the tropical tropopause, while in the GFDL model the tropical tropopause is too warm by 5K in northern summer and 5-10K in northern winter. The tropical temperature structure is mainly determined (at least on a global scale) by

5. SUMMARY AND FURTHER DISCUSSION.

A mass flux convection scheme used at the UK Meteorological Office in both climate and forecast models has been described. The scheme, which can represent both dry and moist convective processes, is designed to simulate the effects of shallow, mid-level and deep convection upon the large-scale flow. The scheme is based upon the concept of representing an ensemble of convective clouds using a 'bulk' one dimensional cloud model. Although a 'bulk' cloud model is used, account is taken of the effects of clouds within the ensemble which detrain at neutral buoyancy at levels lower than the maximum height reached by the parcel (so call 'forced' detrainment described in section (2)). This contrasts to other mass flux schemes which either consider an ensemble of such models (each representing clouds of differing height), such as the complex Arakawa - Schubert scheme or those which consider one type of cloud, for example the scheme proposed by Tiedtke (1988). The closure hypothesis of the scheme is relatively simple, the initial convective mass flux being proportional to the parcel's initial buoyancy on ascent. This is unlike most other convection schemes which apply the constraint of quasi-equilibrium between convection and forcing processes to determine convective rainfall.

Single column model experiments using observational data (GATE, BOMEX, ATEX) show that the scheme is able to represent both deep and shallow convection. Simulating deep convection during GATE, the convection scheme comes into balance with the forcing provided. The heating and drying due to convection are distributed realistically in the vertical while a

the balance between convection and radiation. The relative agreement (compared to similar models) of the 11-layer climate model temperature structure with observations suggests that the interaction between convective and radiative processes is reasonably well modelled.

5. SUMMARY AND FURTHER DISCUSSION.

A mass flux convection scheme used at the UK Meteorological Office in both climate and forecast models has been described. The scheme, which can represent both dry and moist convective processes, is designed to simulate the effects of shallow, mid-level and deep convection upon the large-scale flow. The scheme is based upon the concept of representing an ensemble of convective clouds using a 'bulk' one dimensional cloud model. Although a 'bulk' cloud model is used, account is taken of the effects of clouds within the ensemble which detrain at neutral buoyancy at levels lower than the maximum height reached by the parcel (so call 'forced' detrainment described in section (2)). This contrasts to other mass flux schemes which either consider an ensemble of such models (each representing clouds of differing height), such as the complex Arakawa - Schubert scheme or those which consider one type of cloud, for example the scheme proposed by Tiedtke (1988). The closure hypothesis of the scheme is relatively simple, the initial convective mass flux being proportional to the parcel's initial buoyancy on ascent. This is unlike most other convection schemes which apply the constraint of quasi-equilibrium between convection and forcing processes to determine convective rainfall.

Single column model experiments using observational data (GATE, BOMEX, ATEX) show that the scheme is able to represent both deep and shallow convection. Simulating deep convection during GATE, the convection scheme comes into balance with the forcing provided. The heating and drying due to convection are distributed realistically in the vertical while a

reasonable temperature structure is maintained. However deficiencies exist in the vertical distribution of moisture. It has also been noted that the boundary layer temperature structure is too stable, and that the sub-cloud layer too cold and wet, both due to allowing the evaporation of falling rain only below cloud base. This leads to errors in the magnitude of the simulated surface fluxes. In simulations of shallow convection using BOMEX and ATEX data, the scheme also comes in balance with the forcing with a realistic distribution of convective heating and drying in the vertical. However too much moisture is transported above the inversion and the atmosphere below this is too dry and warm.

Although single column model tests of convection schemes are valuable indicators of a schemes performance, their limitation is that the large-scale forcing is fixed and so cannot evolve in response to the convective forcing. Hence it is necessary to test the scheme in an AGCM to fully ascertain whether it is a reasonable representation of convection.
A study of the time mean tropical circulation in an 11-layer AGCM has been presented. The scheme is able to simulate the main areas of latent heat release in the tropics reasonably well although deficiencies in fields associated with convection were noted.

Both the single column model and AGCM studies presented indicate that the scheme performs well. Thus it would appear possible to represent the effects of an ensemble of convective clouds on the large-scale flow by using a mass flux approach based around a 'bulk' cloud model rather than a more complex scheme with a spectrum of cloud models. The results also give support for the simple closure hypothesis used.

Experiments using GATE data in the single column model provide some insight into the mechanism by which the convection scheme comes into balance with the large-scale forcing. It is not constrained to do so by the closure hypothesis but does so by a modification of the stability of the two lowest convecting layers. The stability of these layers to ascent controls the magnitude of the convective heat release while changes in thermodynamic structure above this control the vertical distribution of the heating. Hence convection interacts with large-scale ascent, surface fluxes and radiation via the thermodynamic structure of the atmosphere. This seems physically reasonable and perhaps a more realistic closure than constraining the convection to follow the forcing as in the quasi-equilibrium approach. The closure of the scheme is robust to changes in the parameters used to specify the initial mass flux. Single column model experiments with the parameter 'c' (eqn(20)) reduced ten fold produce changes of only 1-2K in the simulated temperature structure above the boundary layer (fig 9), the boundary layer becoming more unstable to ascent, compensating the weaker generation of convective mass flux for a given stability. Similar results have been found in AGCM sensitivity experiments (not shown), large changes in the specification of the initial mass flux resulting in only small changes in the distribution of global rainfall and in the temperature structure of the tropical atmosphere.

Work is in progress to improve some of the deficiences commented upon. Changes to correct for the excessive transport of moisture above the boundary layer in cases of shallow convection are being investigated. Also the inclusion of a more complex cloud microphysics to allow a better estimate of convective cloud liquid water path for use in the model's

radiation scheme is being considered. This will also give an improved estimate of the amount of liquid detrained from the cloud. Perhaps the most notable omission in the scheme is the lack of a downdraught representation in the presence of deep convection. Inclusion of such a feature would allow the evaporation of falling precipitation over a much greater depth of the convective layer and also transport low equivalent potential temperature air from the mid-troposphere into the boundary layer. Both these changes will effect the stability of the boundary layer which at present is too stable in the presence of deep convection (fig 6). First results from single column model experiments employing a new convection scheme in which the effects of both updraughts and downdraughts are modelled show an improved simulation of boundary layer structure and surface fluxes.

REFERENCES

Anthes, R.A., 1977 : A cumulus parameterization scheme utilizing a one-dimensional cloud model., Mon. Wea. Rev., 105, pp270-286

Arakawa, A., and Schubert, W.H., 1974 : Interaction of a cumulus cloud ensemble with the large-scale environment, part I., J .Atmos. Sci., 31, pp674-701

Augstein, E., Riehl, H., Ostopoff, F., and Wagner, V., 1973 : Mass and energy transports in an undisturbed Atlantic trade-wind flow., Mon. Wea. Rev., 101, pp101-111

Betts, A.K., and Miller, M.J., 1986 : A new convective adjustment scheme. II : Single column model tests using GATE wave, Bomex and artic air-mass data sets., Quart. J. Roy. Meteor. Soc., 112, pp693-710

Carson, D.J., 1982a : Comments on the sensitivity of numerical simulations to different parametrizations of the boundary layer properties and processes., pp119-153 in Workshop on Planetary boundary layer parametrization, 25-27 November 1981, ECMWF, Reading, UK.

Clarke, R.H., 1970 : Recommended methods for the treatment of the boundary layer in numerical models., Austr. Met. Mag., 18, pp51-73

Cunnington, W.M., and Rowntree, P.R., 1986 : Simulations of the Saharan atmosphere - dependence on moisture and albedo., Quart. J. Roy. Meteor. Soc., 112, pp971-999

Dopplick, T.G., 1970 : Global radiative heating of the Earth's atmosphere., Report N°.24, Planetary circulation project, Dept. Meteor., MIT, 128pp

Dorman, C.E., and Bourke, R.H., 1979 : Precipiataion over the Pacific Ocean, 30°S to 60°N., Mon. Wea. Rev., 107, pp896-910

Emanuel, K.A., 1987 : Large-scale and mesoscale circulations in convectively adjusted atmospheres., pp323-348 in Workshop on Diabatic forcing, 30 Nov - 2 Dec 1987, ECMWF, Reading, UK.

Graham, N.E. and Barnett, T.P., 1987 : Sea surface temperature, surface wind divergence, and convection over tropical oceans., Science, 283, pp657-659

Gregory, D., and Miller, M.J., 1989 : A numerical study of the parametrisation of deep tropical convection., to appear in the October 1989 (115) issue of Quart. J. Roy. Meteor. Soc.

Holland, J.Z., and Rasmusson, E.M., 1973 : Measurements of the atmospheric mass, energy and momentum budgets over a 500 kilometer square of tropical ocean., Mon. Wea. Rev., 101, pp44-55

Jaeger, L., 1976 : Monatskarten des Niederschlages für die ganze Erde., Ber. Dtsch. Wetterd., Offenbach/Main, N°. 139, Vol. 19, 38pp

Johnson, R.H., 1980 : Diagnosis of convective and mesoscale motions during phase III OF GATE., J. Atmos. Sci., 37, pp733-753

Kessler, E., 1969 : On the distribution and continuity of water substance in atmospheric circulations., Met. Mon., (Amer. Met. Soc.), 10, N°. 32.

Kilonsky, B.J., and Ramage, C.S., 1976 : A technique for estimating tropical open-ocean rainfall from staellite observations., J. Appl. Met., 15, pp972-975

Krügermeyer, L., 1976 : Vertical transports of momentum, sensible and latent heat from profiles at the tropical Atlantic during ATEX., "Meteor" Forschungsergeben., Berlin, Reihe B, N°. 11, pp51-77

Kuo, H.L., 1974 : Further studies of the parameterization of the influence of cumulus convection on large-scale flow., J .Atmos. Sci., 31, pp1232-1240

Lord, S.J., and Arakawa, A., 1980 : Interaction of a cumulus cloud ensemble with the large-scale environment, part II., J .Atmos. Sci., 37, pp2677-2692

Ludlam, F.H., 1980 : Clouds and Storms., Pennsylvania State Univ., 407pp plus plates

Lyne, W.H., and Rowntree, P.R., 1976 : Development of a convective parametrization using GATE data., Met O 20 Technical Note II/70, Meteorological Office, Bracknell, UK.

Miller, D.B., and Feddes, R.G., 1971 : Global atlas of relative cloud cover 1967-70 based on data from meteorological satellites., Washington : N.O.A.A., N.E.S.S., 237pp

Nitta, T., 1978 : A diagnostic study of the interaction of cumulus updrafts and downdrafts with large-scale motions in GATE., J. Meteor. Soc. Japan, 56, pp232-241

Ooyama, K., 1971 : A theory on parameterization of cumulus convection., J. Met. Soc. Jap., 49(Special Issue), pp744-756

Reed, R.K., and Elliott, W.P., 1979 : New precipitation maps for the North Atlantic and North Pacific Oceans., J. Geoph. Res., 84, pp7839-7846

Richards, P.J.R., 1980 : An objective assessment of specifications of boundary-layer eddy diffusion coefficients., Met O 20 Technical Note N°. II/140, Meteorological Office, Bracknell, UK

Rowntree, P.R., and Cattle, H. (editors), 1983 : The Meteorological Office GATE modelling experiment., Meteorological Office Scientific Paper N°.40, HMSO, London.

Schlesinger, M.E. and Mitchell, J.F.B., 1985 : Model projections of the equilibrium climatic response to increased carbon dioxide., pp81-147 in 'Projecting the Climatic Effects of Increasing Carbon Dioxide', edited by M.C. Mac-Cracken and F.M. Luther, U.S. Department of Energy, Washington, D.C.

Simpson, J., 1971 : On cumulus entrainment and one dimensional models., J. Atmos. Sci., 28, pp449-455

Simpson, J., and Wiggert, V., 1969 : Models of precipitating cumulus towers., Mon. Wea. Rev., 97. pp471-489

Slingo, A., 1985 : Handbook of the Meteorological Office 11-layer atmospheric general circulation model. Volume 1 : Model description., Dynamical Climatology Technical Note N°.29, Meteorological Office, Bracknell, UK.

Slingo, A., and Pearson, D.W., 1987 : A comparison of the impact of an envelope orography and of a parametrization of orographic gravity-wave drag on model simulations., Quart. J. Roy. Meteor. Soc., 113, pp847-870

Slingo, A., Wilderspin, R.C., and Smith, R.N.B., 1989 : The effect of improved physical parametrizations on simulations of cloudiness and the Earth's radiation budget., Submitted to J. Geophys. Res.

Taylor, R.C., 1973 : An atlas of Pacific islands rainfall., Rep. HIG-73-9, Hawaii Institute of Geophysics, 7pp + 13 figures

Thompson, R.M., Payne, S.W., Recker, E.E., and Reed, R.J., 1979 : Structure and properties of synoptic-scale wave disturbances in the intertropical convergence zone of the eastern Atlantic., J .Atmos. Sci., 36, pp53-72

Tiedtke, M., 1988 : A comprehensive massflux scheme for cumulus parameterization in large-scale models : theoretical basis and verification on single column model data sets from field experiments., Submitted to J. Atmos. Sci.

Yanai, M., Esbensen, S., and Chu, J.-H., 1973 : Determination of bulk properties of tropical cloud clusters from large-scale heat and moisture budgets., J .Atmos. Sci., 30, pp611-627

LIST OF FIGURES

Fig 1 Discretisation of the convection scheme in the vertical

Fig 2 Initial sounding for GATE experiments (based on category one of TPRR (1979)

Fig 3 Large-scale temperature (———) and moisture forcing (- - -) supplied to model for GATE experiments plus radiative cooling (-·-·-) calculated by the model (averages over wave cycle 2 through 6).

Fig 4 Comparison of simulated surface rainfall (———) with moisture forcing due to large-scale and surface processes (-···-) and the observed rainfall (- - -). Values are averaged over 10 hour periods. Model values averaged over wave cycle 2 through 6.

Fig 5 Comparison of modelled and observed evolution of (a) Q1 (K/day)and (b) Q2 (g/kg/day). Modelled values are composited over wave cycles 2 through 6.

Fig 6 Comparison of the simulated wave average thermodynamic profiles (wave cycles 2 through 6) (———) with observations (- - -).

Fig 7 Deviation of wave average T and q from observations for wave cycle 1 (———) and wave cycles 2 through 6 (- - -)

Fig 8 Comparison of convective heating profiles from one time step integrations of the single column model using the wave averaged observed (———) and modelled (- - -) thermodynamic structure. The wave averaged forcing (-·-·-) is also shown.

Fig 9 Deviation of wave average T (wave cycle 2 through 6) from observations for sensitivity experiments.
——— : standard scheme. - - - : xpmin=2g/kg.
····· : entrainment doubled. -·-·- : $c=3.33\times10^{-5}$

Fig 10 Comparison of model (———) and observed thermodynamic (- - -) profiles for BOMEX. Modelled values averaged over 6 to 24 hours.

Fig 11 (a) Heating and (b) moistening due to convective (- - -) and boundary layer transports (-·-·-) and large-scale (———) and radiative forcing (·····) averaged between 6 and 24 hours of the BOMEX experiment.

Fig 12 Comparison of modelled total diabatic heating (———) with that observed during BOMEX (- - -)

Fig 13 Comparison of model (———) and observed thermodynamic (- - -) profiles for ATEX. Modelled values averaged over 6 to 24 hours.

Fig 14 (a) Heating and (b) moistening due to convective (- - -) and boundary layer transports (-·-·-) and large-scale (———) and radiative forcing (·····) averaged between 6 and 24 hours of the ATEX experiment.

Fig 15 Comparison of modelled rainfall from a four year integration of an 11-layer AGCM with the observed climatology of Jaeger for (a) Winter, (b)Summer

Fig 16 Modelled velocity potential ($\times 10^6$) and divergent wind at 200mb for a four year integration of an 11-layer AGCM and difference from an observed climatology (1982 - 1983) obtained from the Meteorological Office archive of operational analyses, for (a) Winter, (b) Summer

Fig 17 Wind at 850mb from a four year integration of an 11 - layer climate model compared with an observed climatology (as fig 16) for (a) Winter, (b) Summer

Fig 18 Plot of OLR against SST for convective grid points between 30°N and 30°S for a four year integration of an 11 - layer AGCM (———) compared with the results of an observational study (Graham and Barnett (1987)) (- - -).

Fig 19 Height - latitude diagrams of zonal mean temperature for the tropics and sub-tropics of a four year integration of an 11 - layer AGCM and difference from an observed climatology (as fig 16) for (a) Winter, (b) Summer .

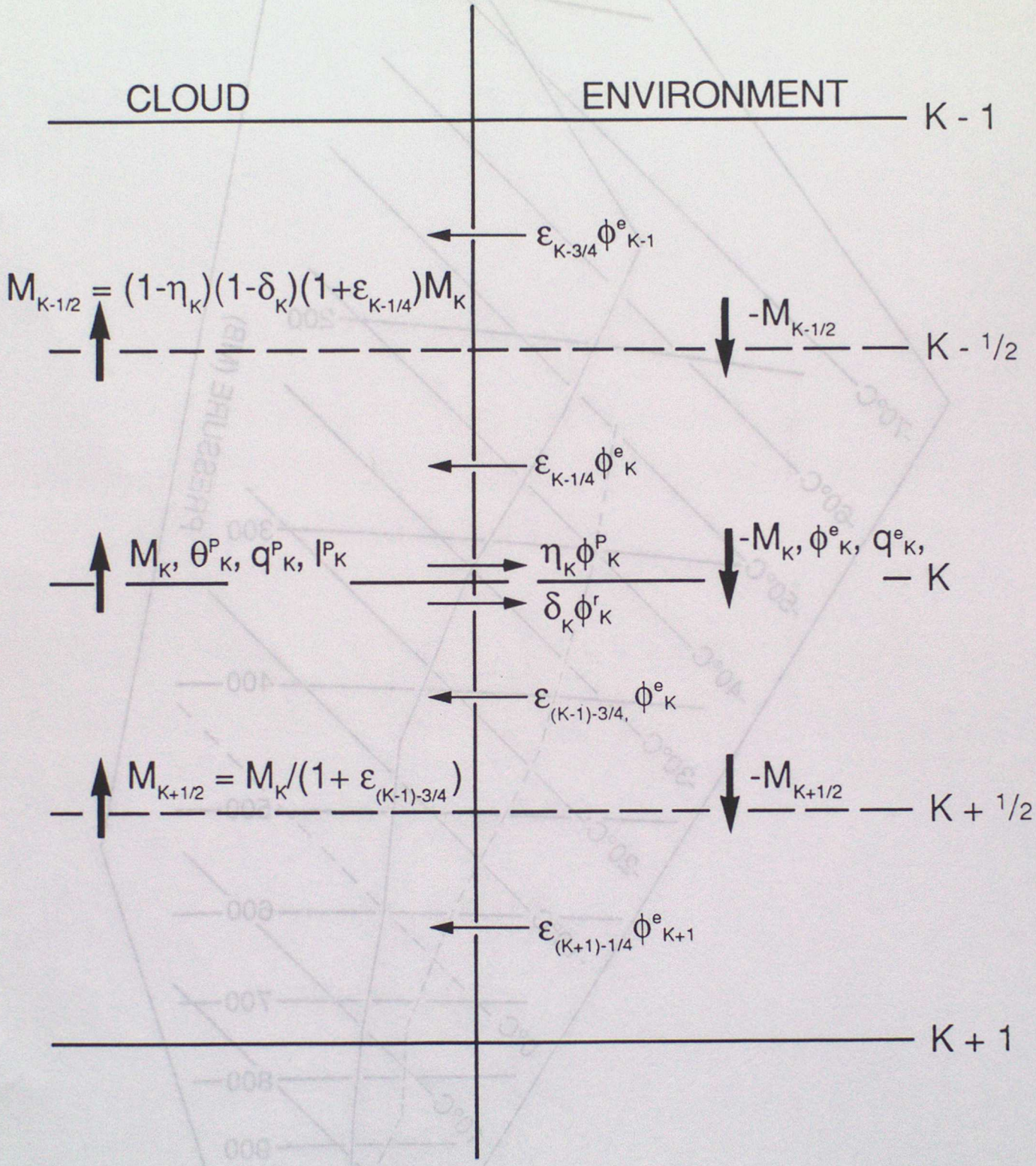

Figure 1. Discretisation of the covection scheme in the vertical.

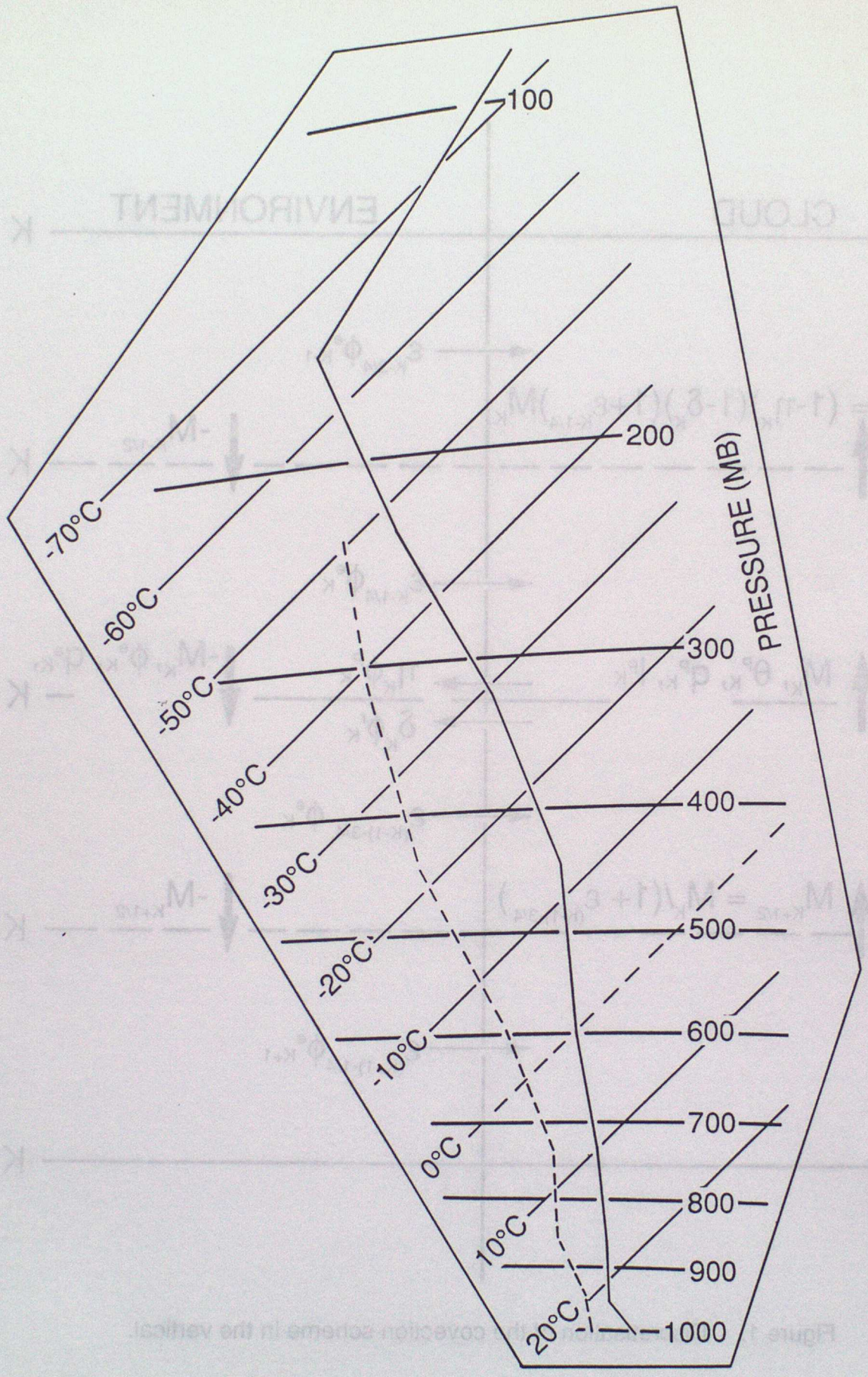

Figure 2. Initial sounding for GATE experiments (based on category one of TPRR (1979)).

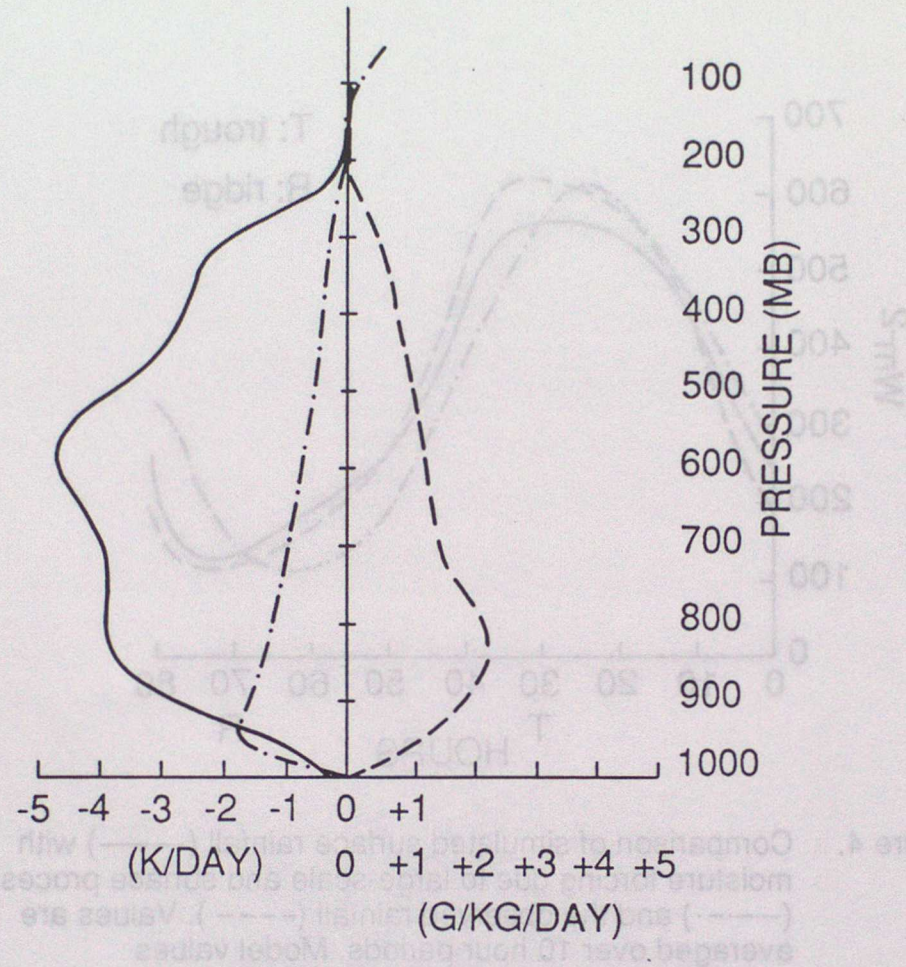

Figure 3. Large-scale temperature (———) and moisture forcing (– – – –) supplied to model for GATE experiments plus radiative cooling (—·—·—) calculated by the model (averages over wave cycle 2 through 6).

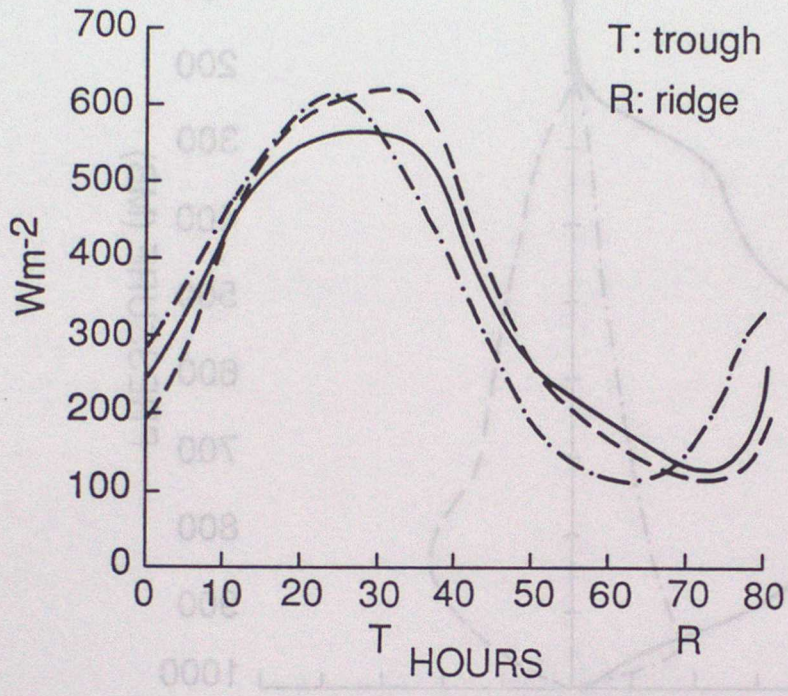

Figure 4. Comparison of simulated surface rainfall (——) with moisture forcing due to large-scale and surface processes (—·—·—·) and the observed rainfall (- - - -). Values are averaged over 10 hour periods. Model values averaged over wave cycle 2 through 6.

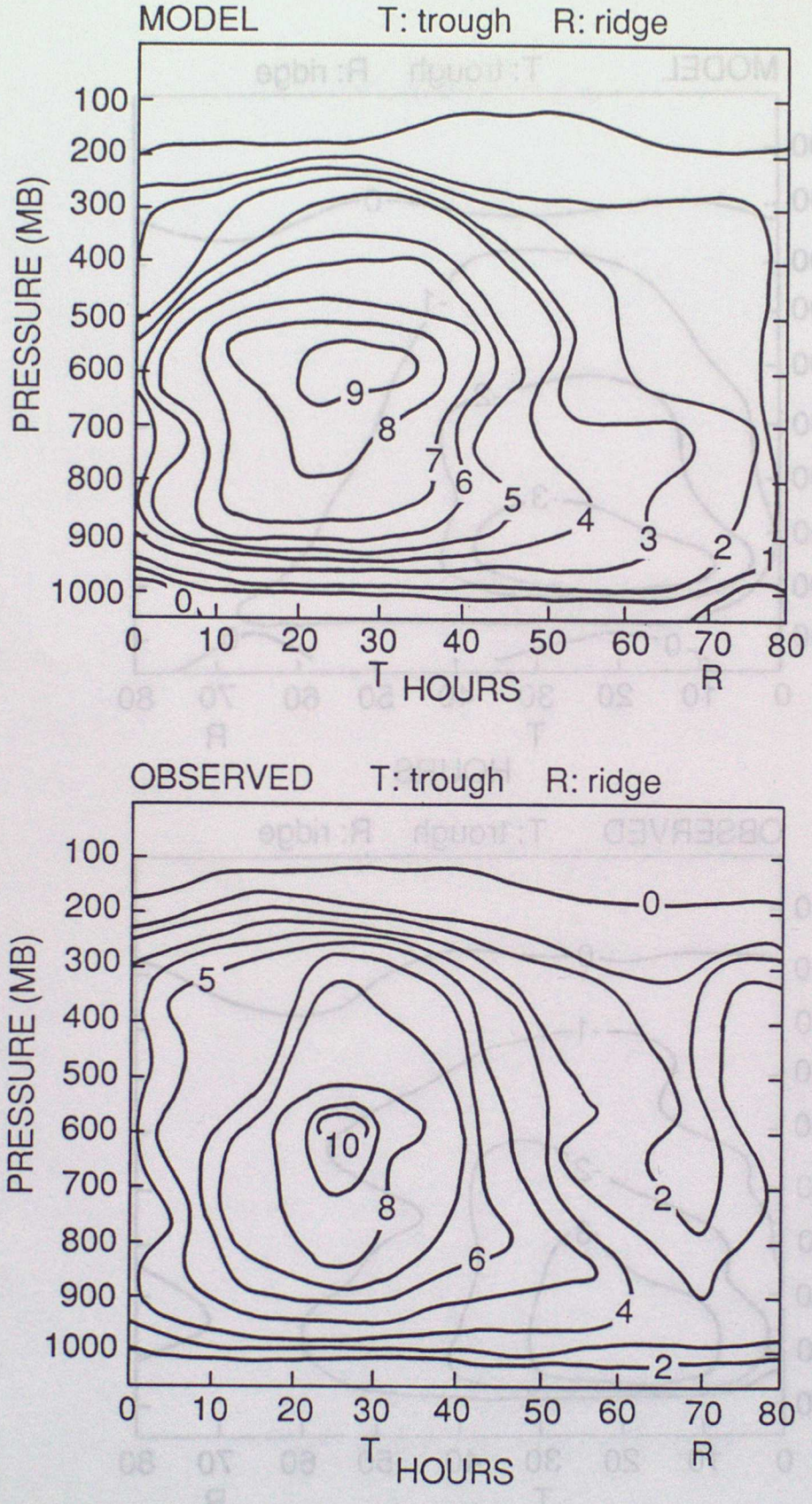

Figure 5a. Comparison of modelled and observed evolution of Q1 (K/day). Modelled values are composited over wave cycles 2 through 6.

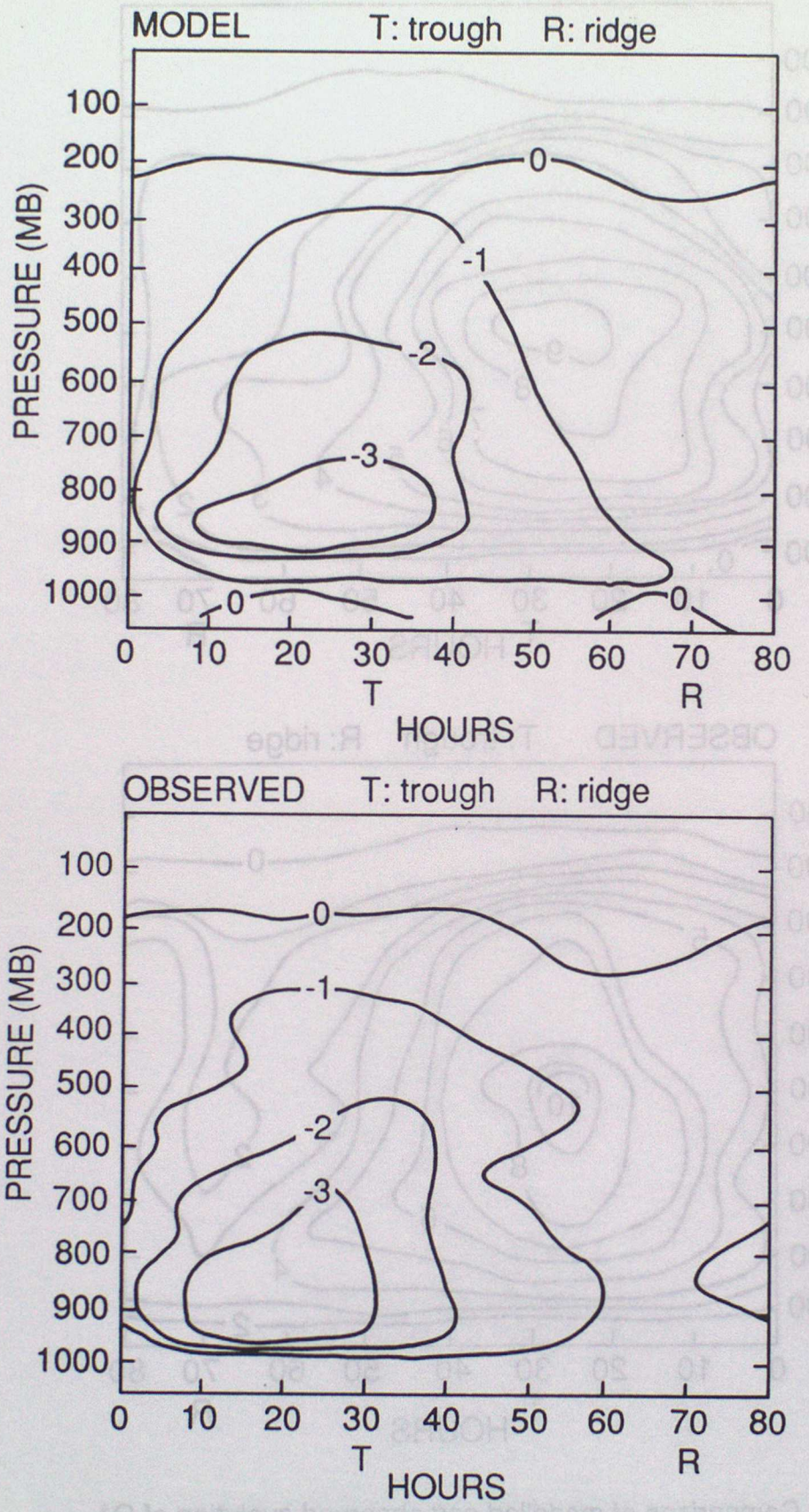

Figure 5b. Comparison of modelled and observed evolution of Q2 (g/kg/day). Modelled values are composited over wave cycles 2 through 6.

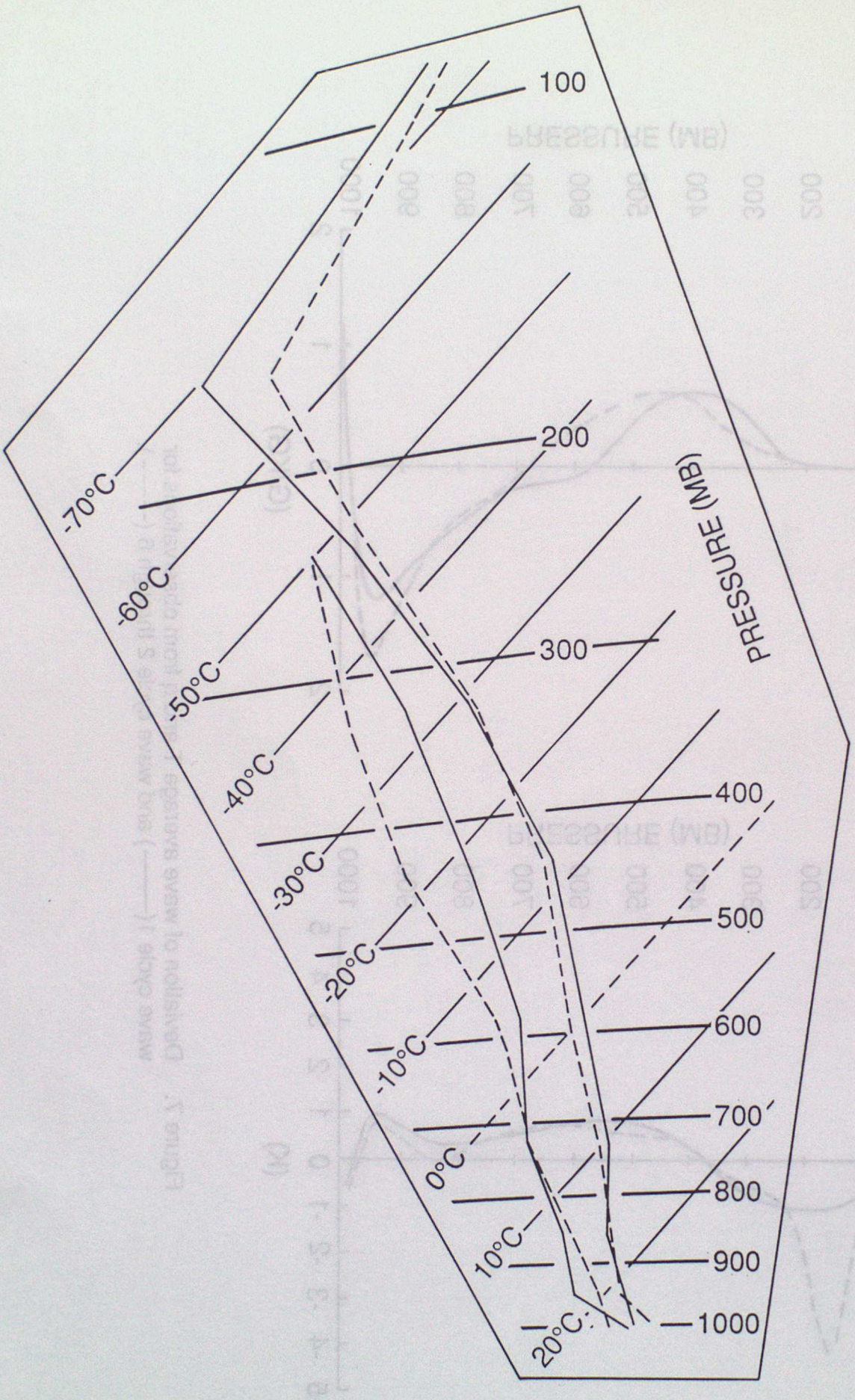

Figure 6. Comparison of the simulated wave average thermodynamic profiles (wave cycles 2 through 6) (——) observations (----).

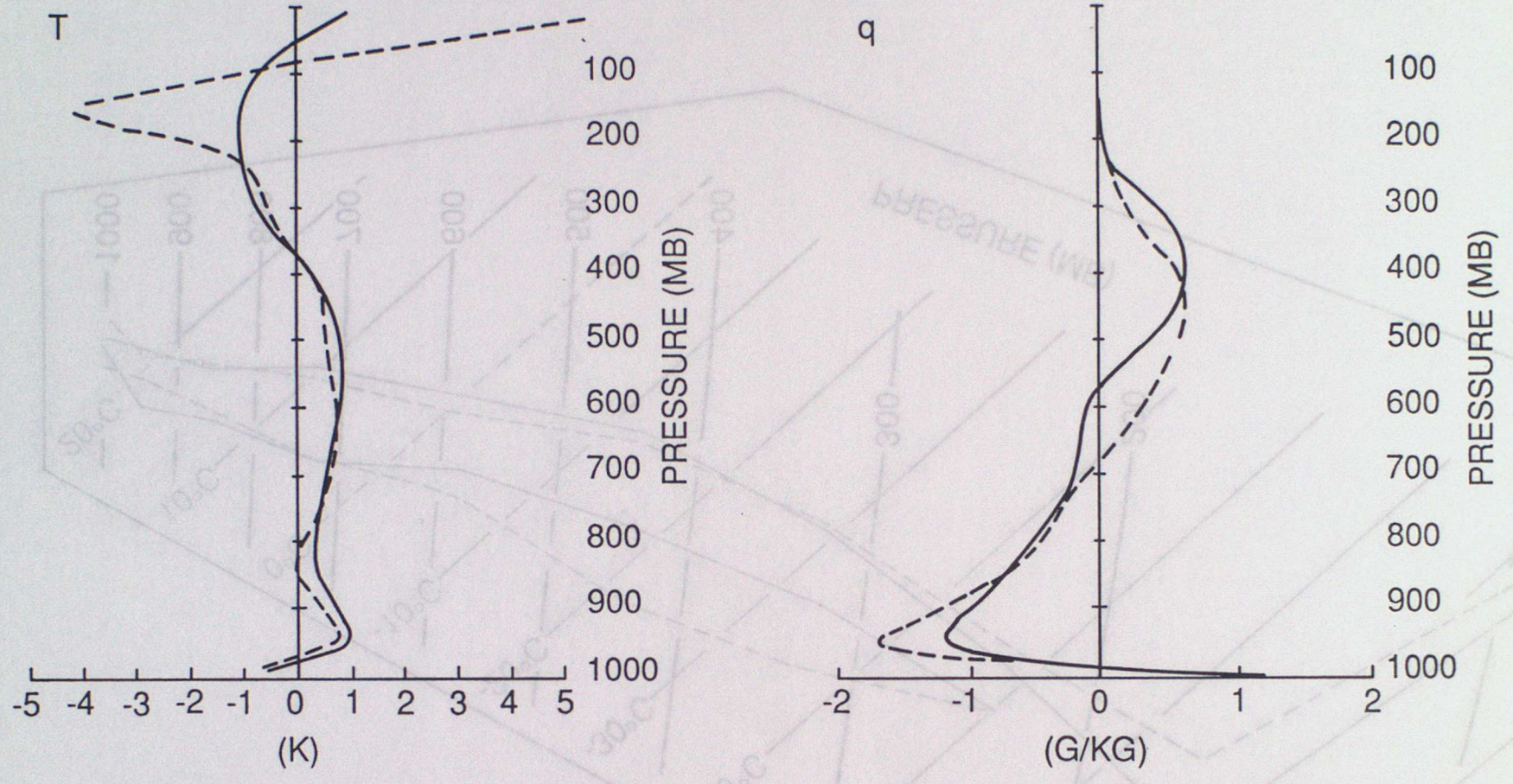

Figure 7. Deviation of wave average T and q from observations for wave cycle 1(———) and wave cycle 2 through 6 (-----).

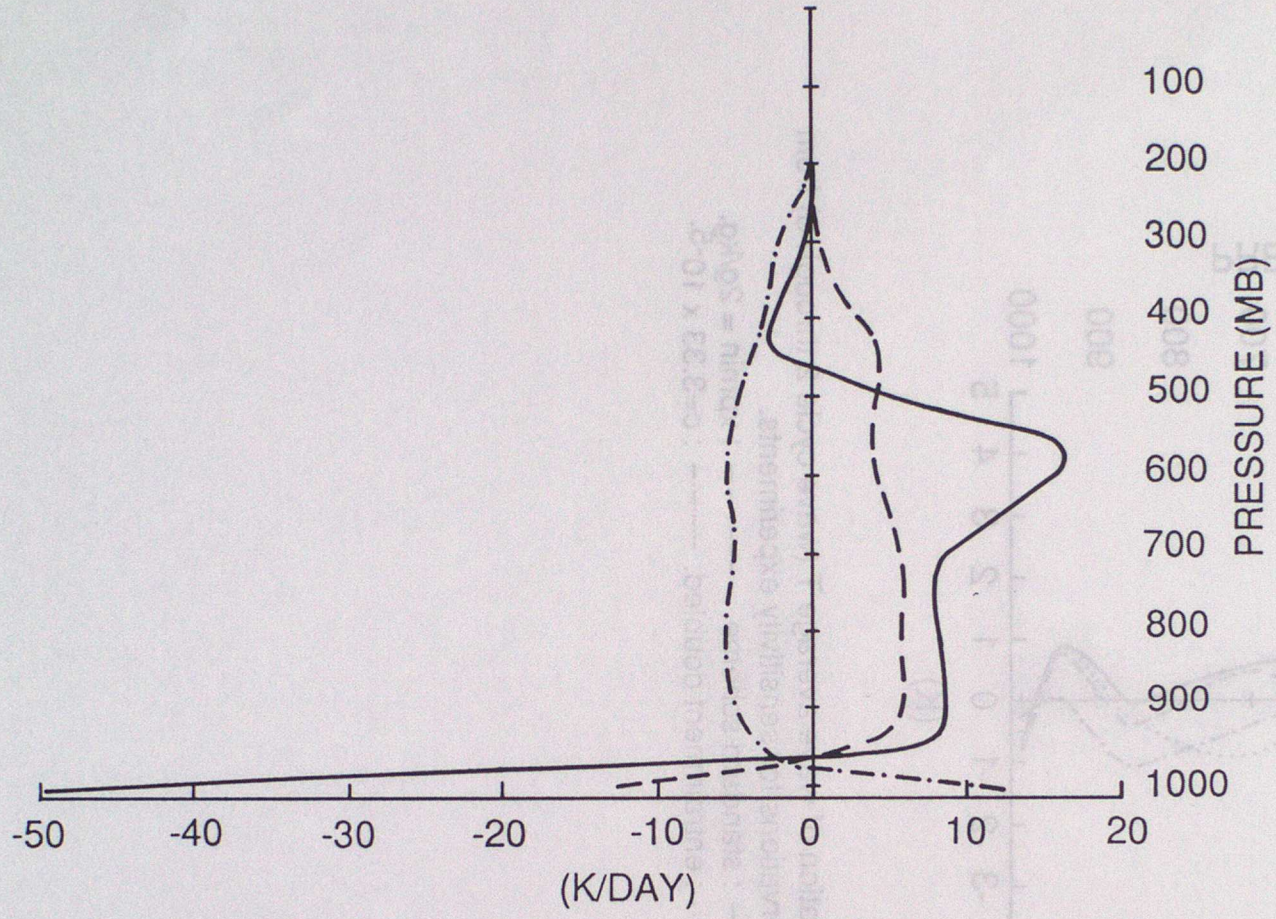

Figure 8. Comparison of convective heating profiles from one time step integrations of the single column model using the wave averaged observed (———) and modelled (- - - -) thermodynamic structure. The wave averaged forcing (-·-·-·) is also shown.

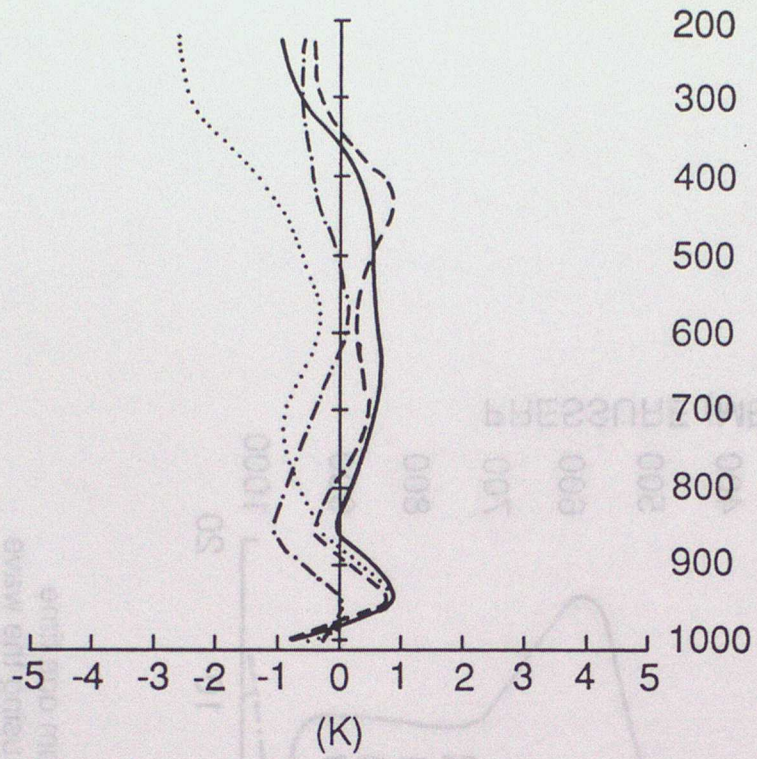

Figure 9. Deviation of wave average T (wave cycle 2 through 6) from observations for sensitivity experiments.
—— : standard scheme. ------ : xpmin = 2g/kg.
····· : entrainment doubled. -·-·-· : $c=3.33 \times 10^{-5}$.

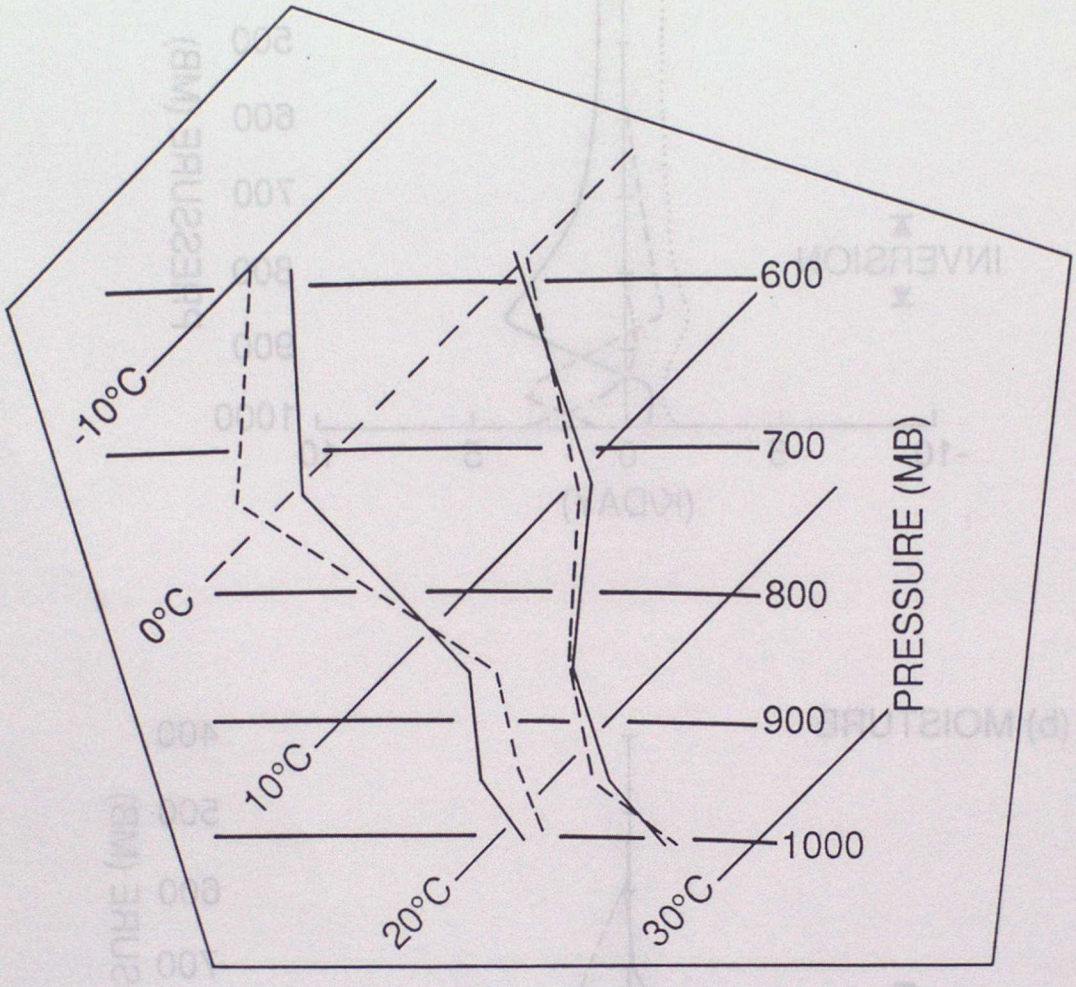

Figure 10. Comparison of model (———) and observed thermodynamic (- - - - -) profiles for BOMEX. Modelled values averaged over 6 to 24 hours.

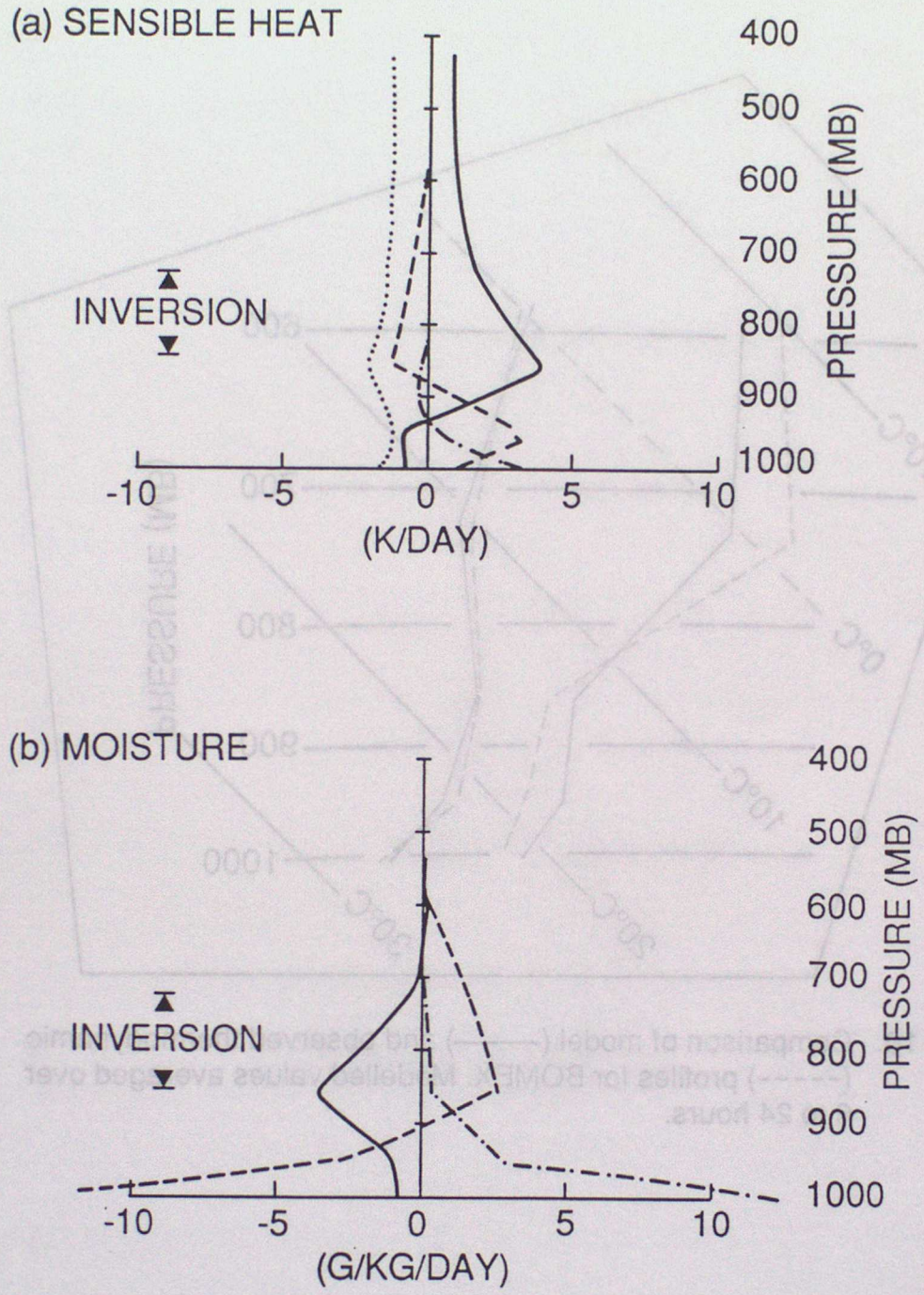

Figure 11. (a) Heating and (b) moistening due to convective (-----) and boundary layer transports (-·-·-·-) and large-scale (———) and radiative forcing (·····) averaged between 6 and 24 hours of the BOMEX experiment.

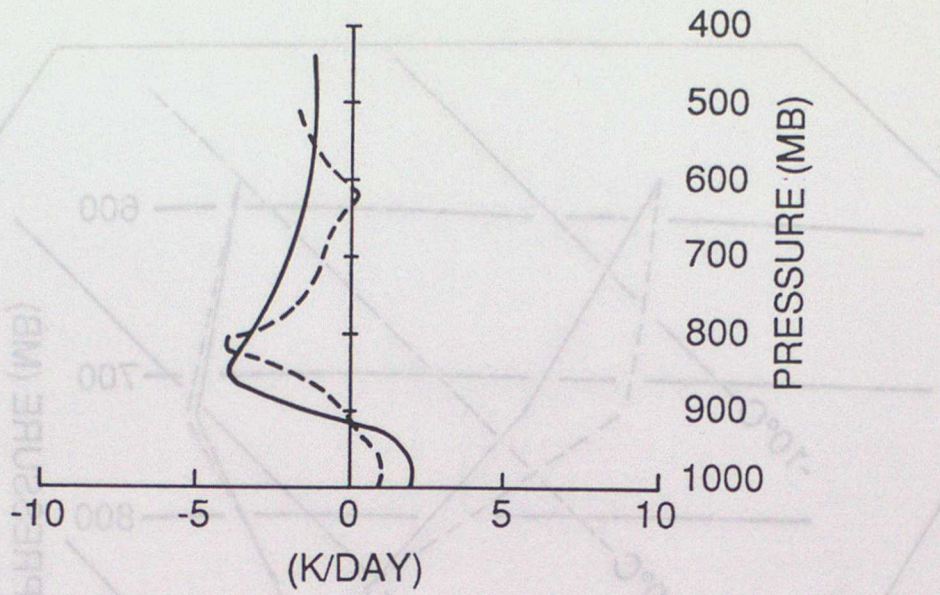

Figure 12. Comparison of modelled total diabatic heating (———) with that observed during BOMEX (- - - - -).

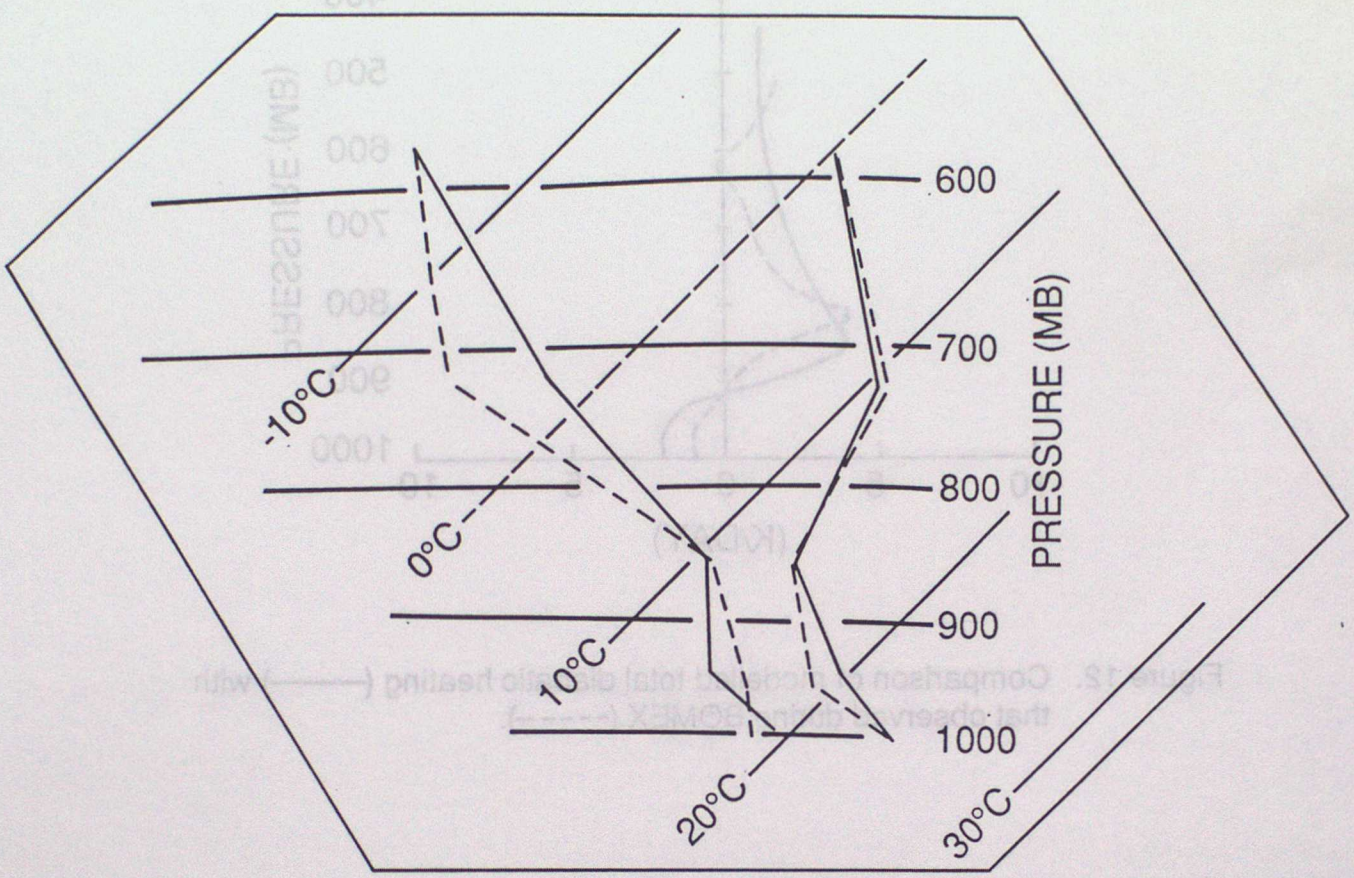

Figure 13. Comparison of model (——) and observed thermodynamic (-----) profiles for ATEX. Modelled values averaged over 6 to 24 hours.

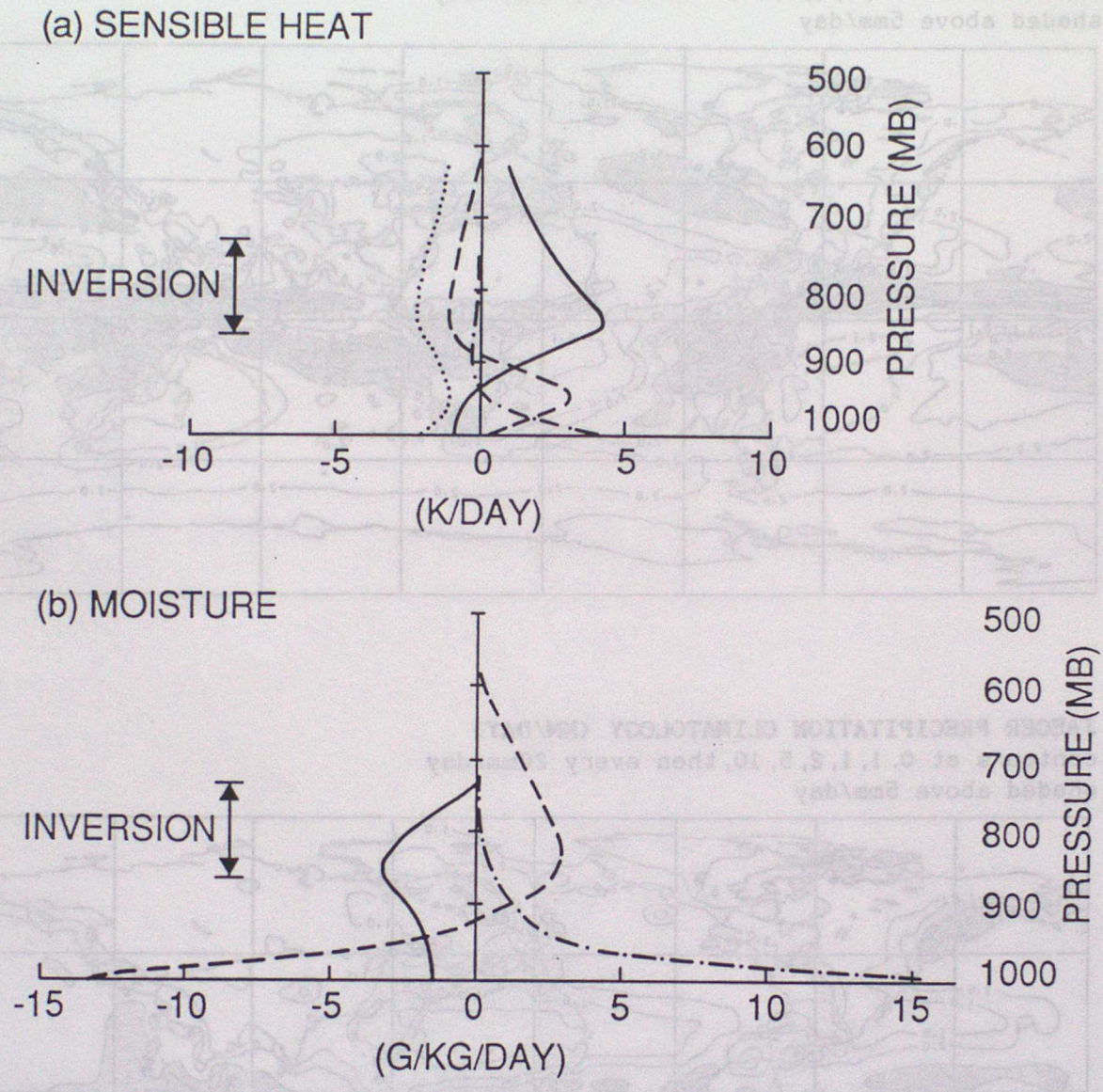

Figure 14. (a) Heating and (b) moistening due to convective (- - - - -) and boundary layer transports (—·—·—·) and large-scale (———) and radiative forcing (·····) averaged between 6 and 24 hours of the ATEX experiment.

(a) **WINTER**

MODEL TOTAL PRECIPITATION (MM/DAY)
contours at 0.1, 1, 2, 5, 10, then every 20mm/day
shaded above 5mm/day

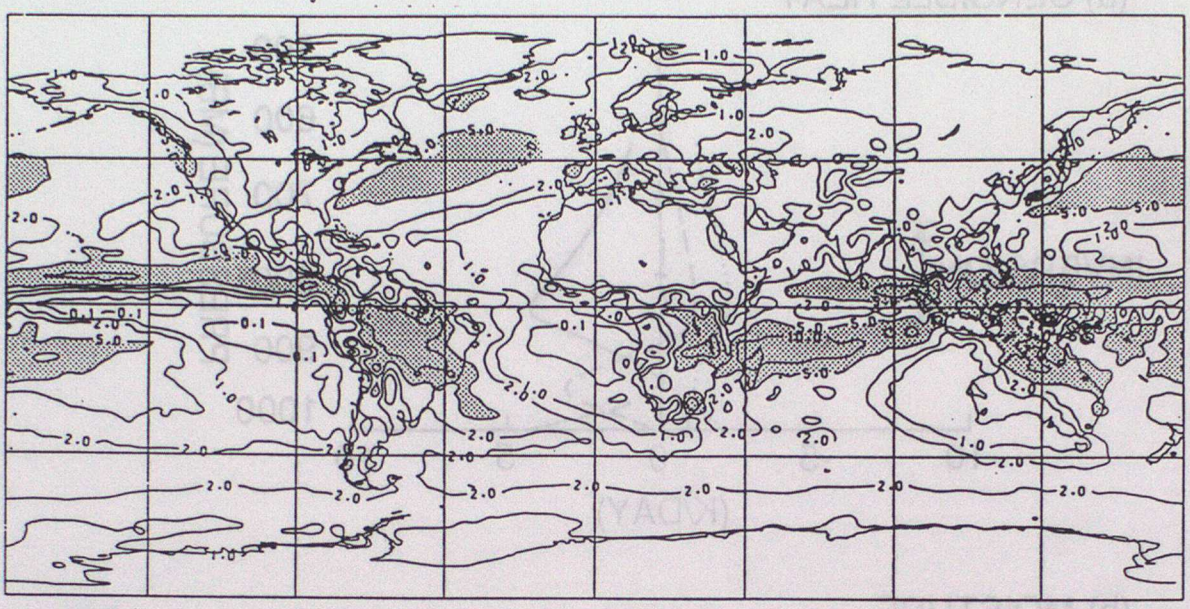

JAEGER PRECIPITATION CLIMATOLOGY (MM/DAY)
contours at 0.1, 1, 2, 5, 10, then every 20mm/day
shaded above 5mm/day

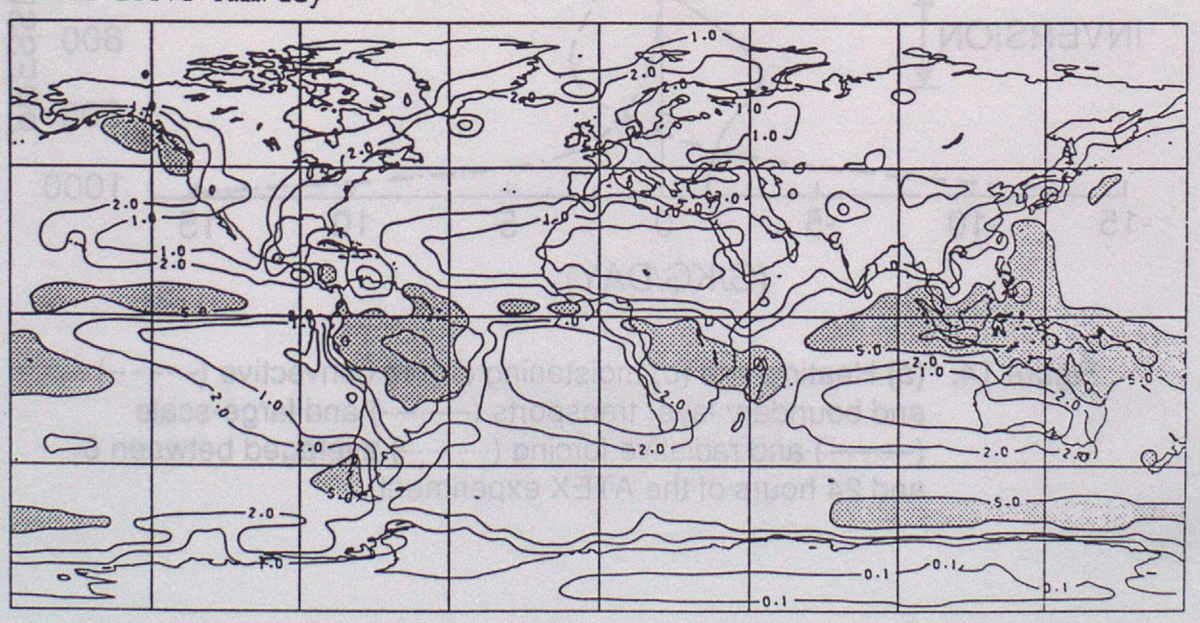

Fig 15a Comparison of modelled rainfall from a four year integration of an 11-layer AGCM with the observed climatology of Jaeger for Winter.

(b) SUMMER

MODEL TOTAL PRECIPITATION (MM/DAY)
contours at 0.1, 1, 2, 5, 10, then every 20mm/day
shaded above 5mm/day

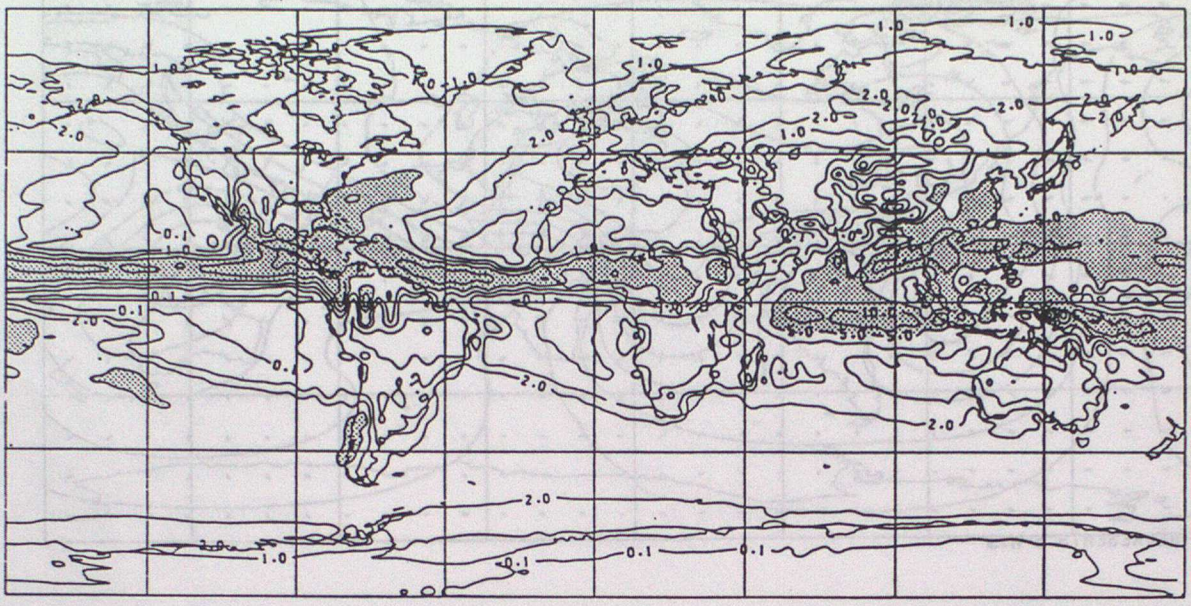

JAEGER PRECIPITATION CLIMATOLOGY (MM/DAY)
contours at 0.1, 1, 2, 5, 10, then every 20mm/day
shaded above 5mm/day

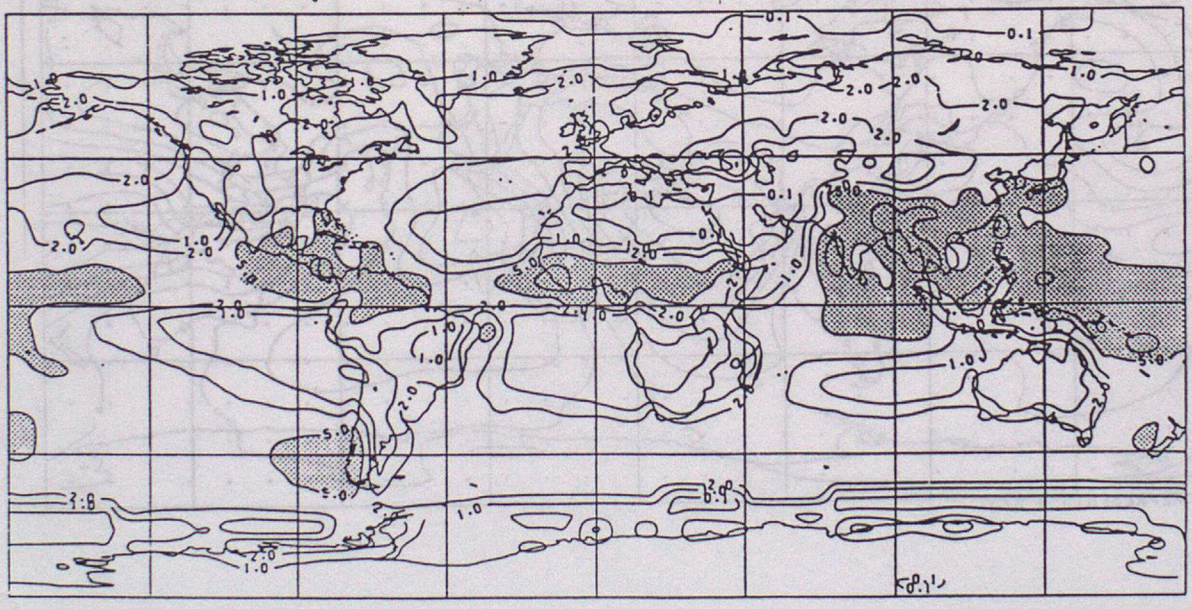

Fig 15b Comparison of modelled rainfall from a four year integration of an 11-layer AGCM with the observed climatology of Jaeger for Summer.

(a) WINTER

MODEL 200MB VELOCITY POTENTIAL ($\times 10^6$) AND DIVERGENT WIND

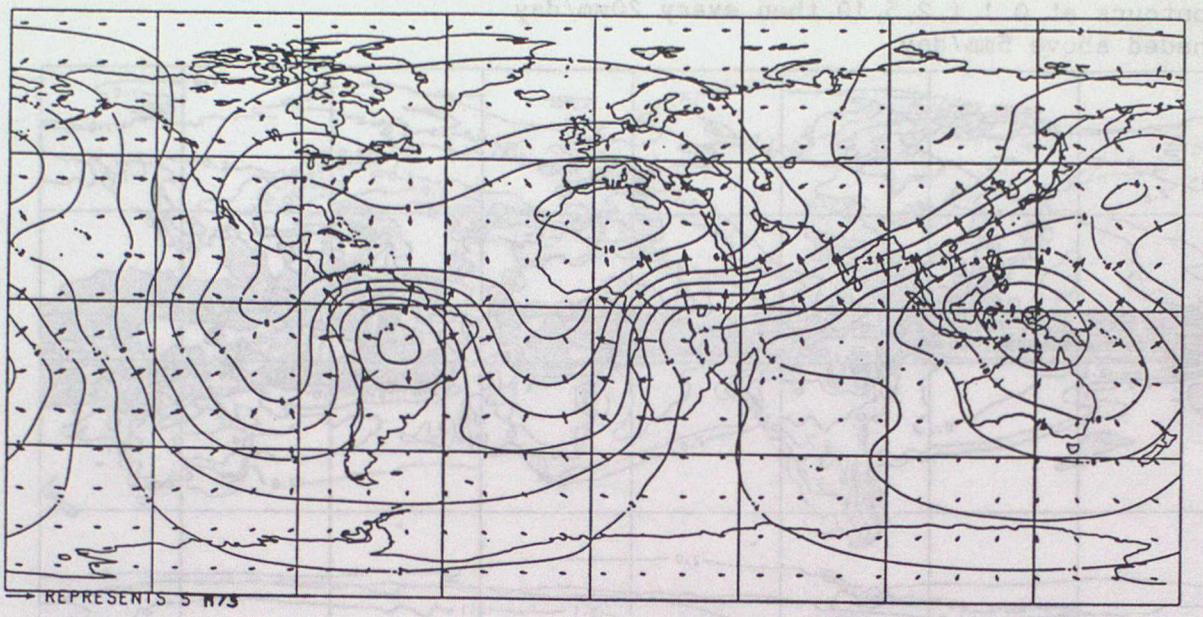

MODEL - OBSERVED
200MB VELOCITY POTENTIAL ($\times 10^6$) AND DIVERGENT WIND

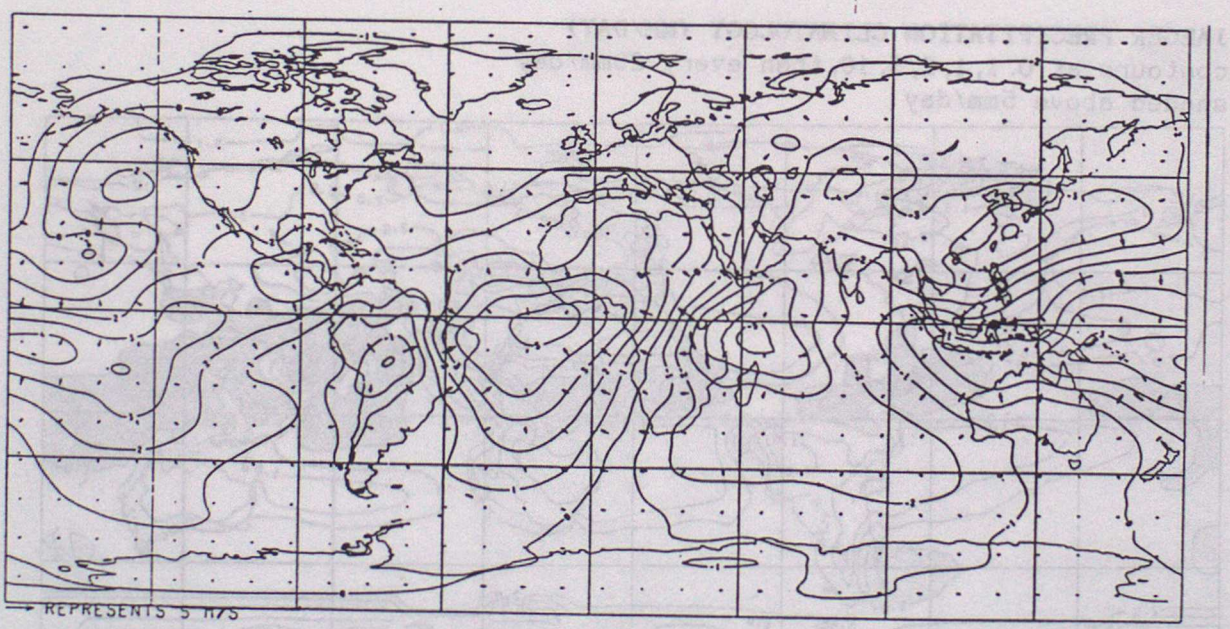

Fig 16a Modelled velocity potential ($\times 10^6$) and divergent wind at 200mb for a four year integration of an 11-layer AGCM and difference from an observed climatology (1982-1983) obtained from the Meteorological Office archive of operational analyses for Winter

(b) SUMMER

MODEL 200MB VELOCITY POTENTIAL ($\times 10^6$) AND DIVERGENT WIND

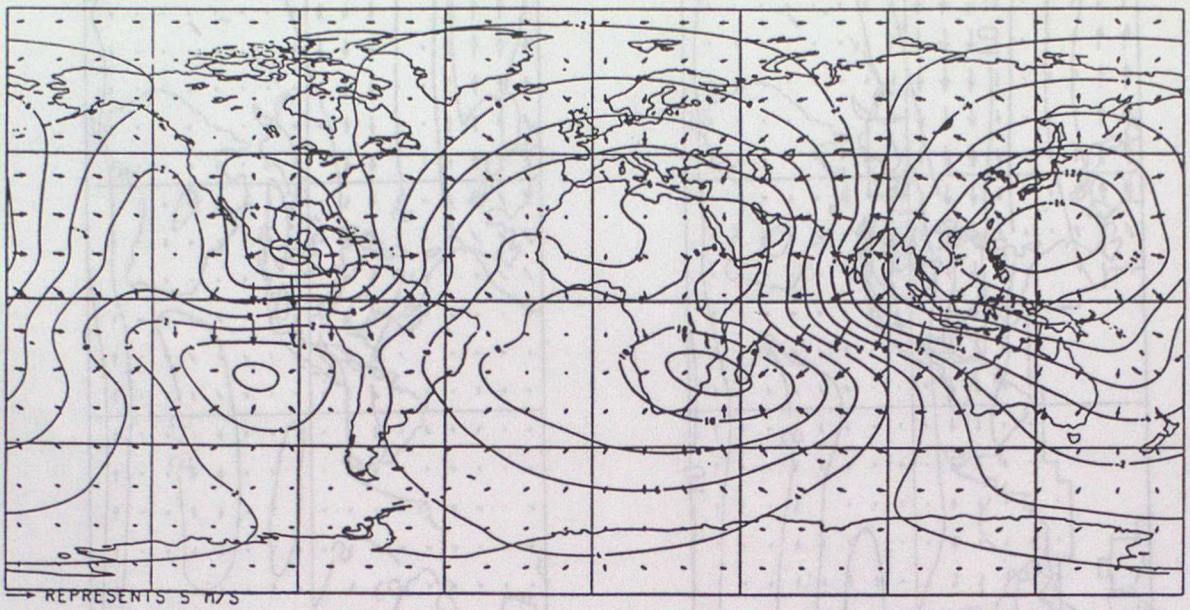

MODEL - OBSERVED
200MB VELOCITY POTENTIAL ($\times 10^6$) AND DIVERGENT WIND

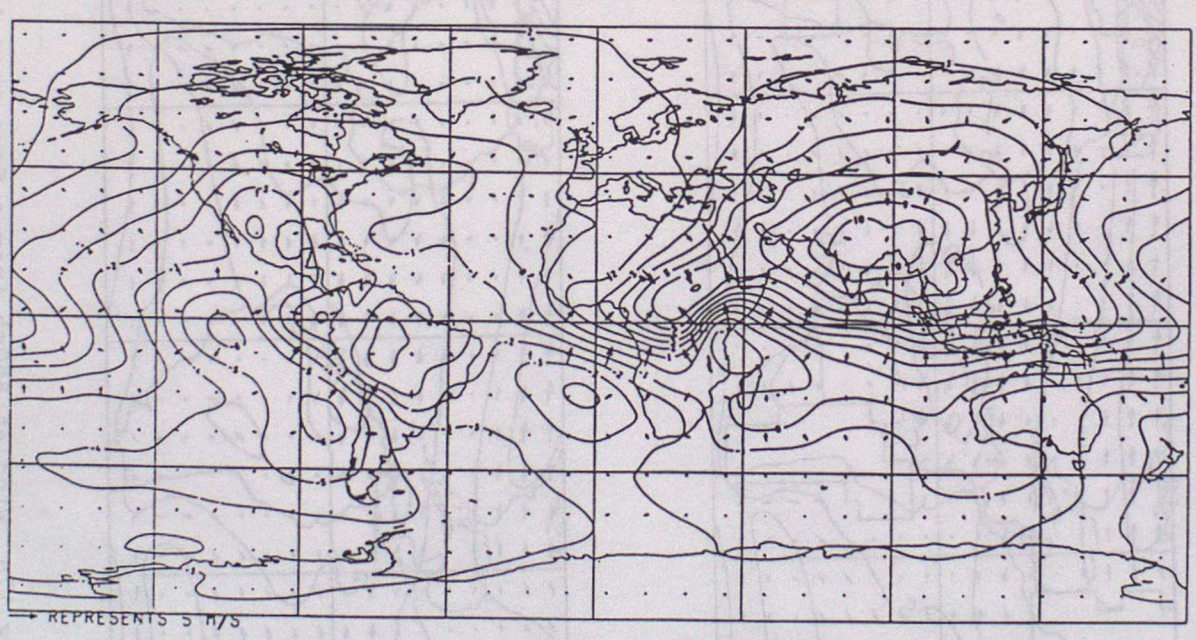

Fig 16b Modelled velocity potential ($\times 10^6$) and divergent wind at 200mb for a four year integration of an 11-layer AGCM and difference from an observed climatology (1982-1983) obtained from the Meteorological Office archive of operational analyses for Summer.

(a) WINTER

MODEL 850MB WIND

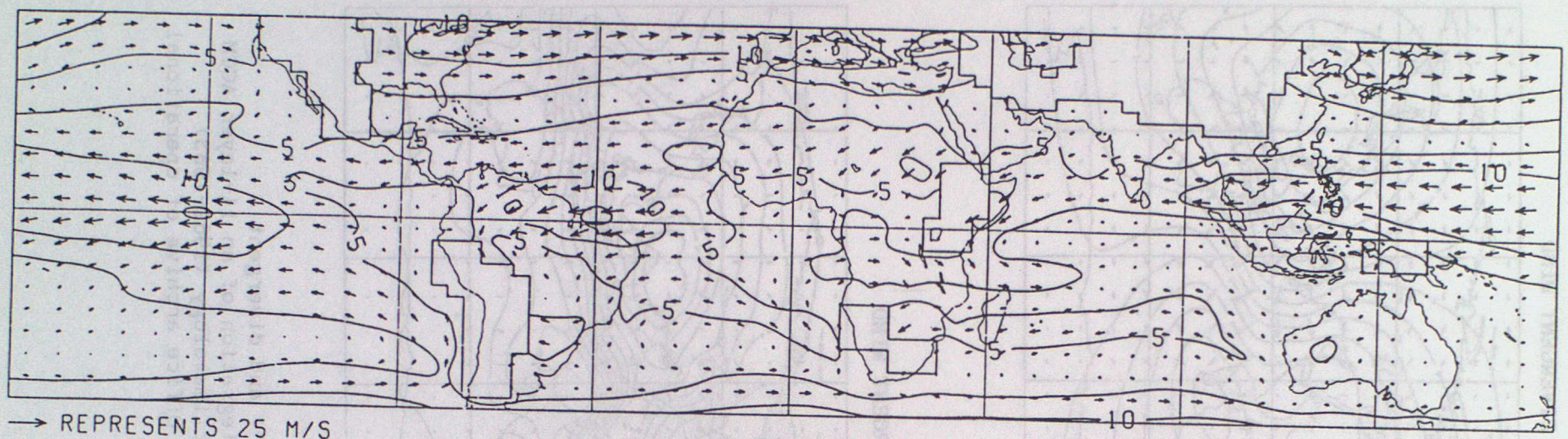

OBSERVED 850MB WIND

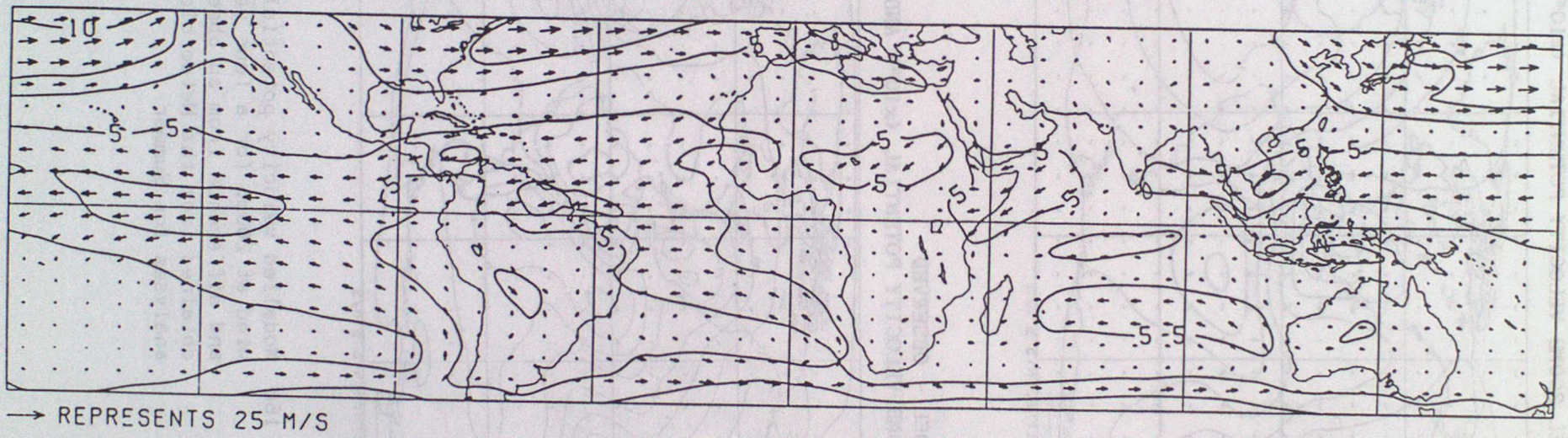

Fig 17a Wind at 850mb from a four year integration of an 11-layer climate model compared with an observed climatology (as fig 16) for winter

(b) SUMMER

MODEL 850MB WIND

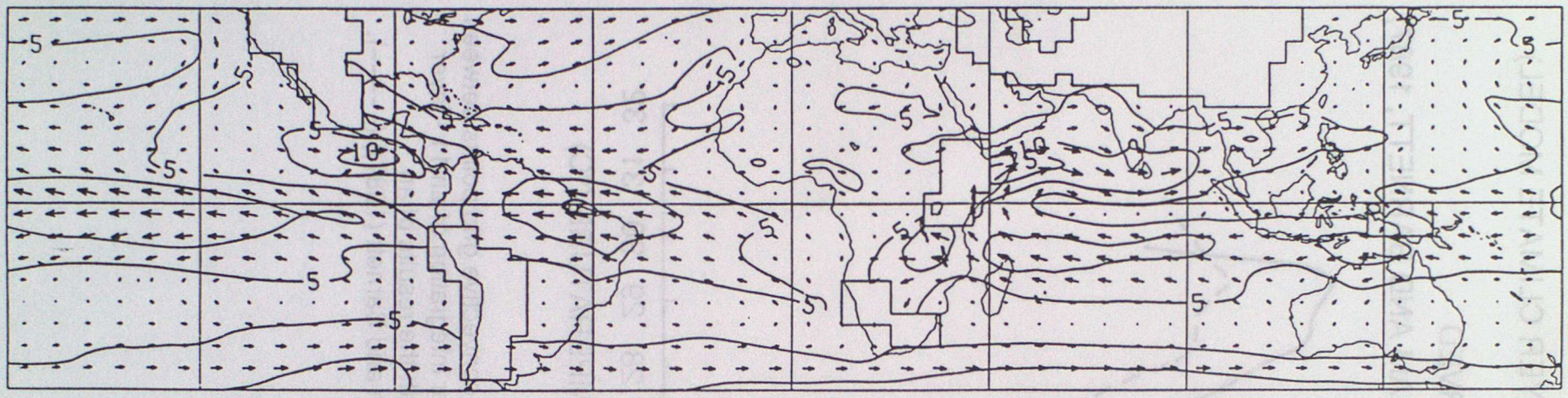

→ REPRESENTS 25 M/S

OBSERVED 850MB WIND

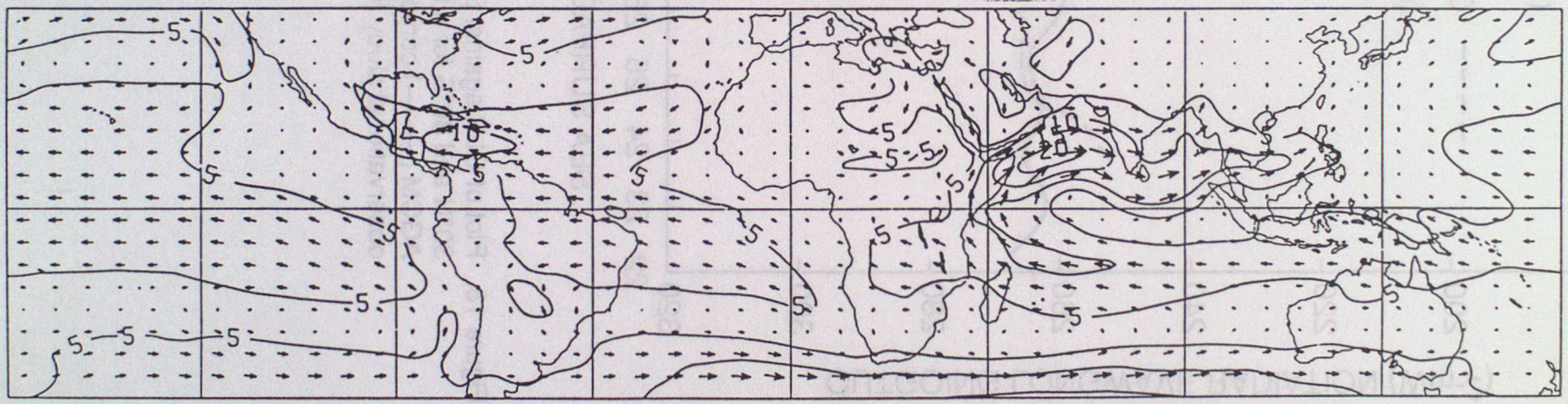

→ REPRESENTS 25 M/S

Fig 17b Wind at 850mb from a four year integration of an 11-layer climate model compared with an observed climatology (as fig 16) for summer.

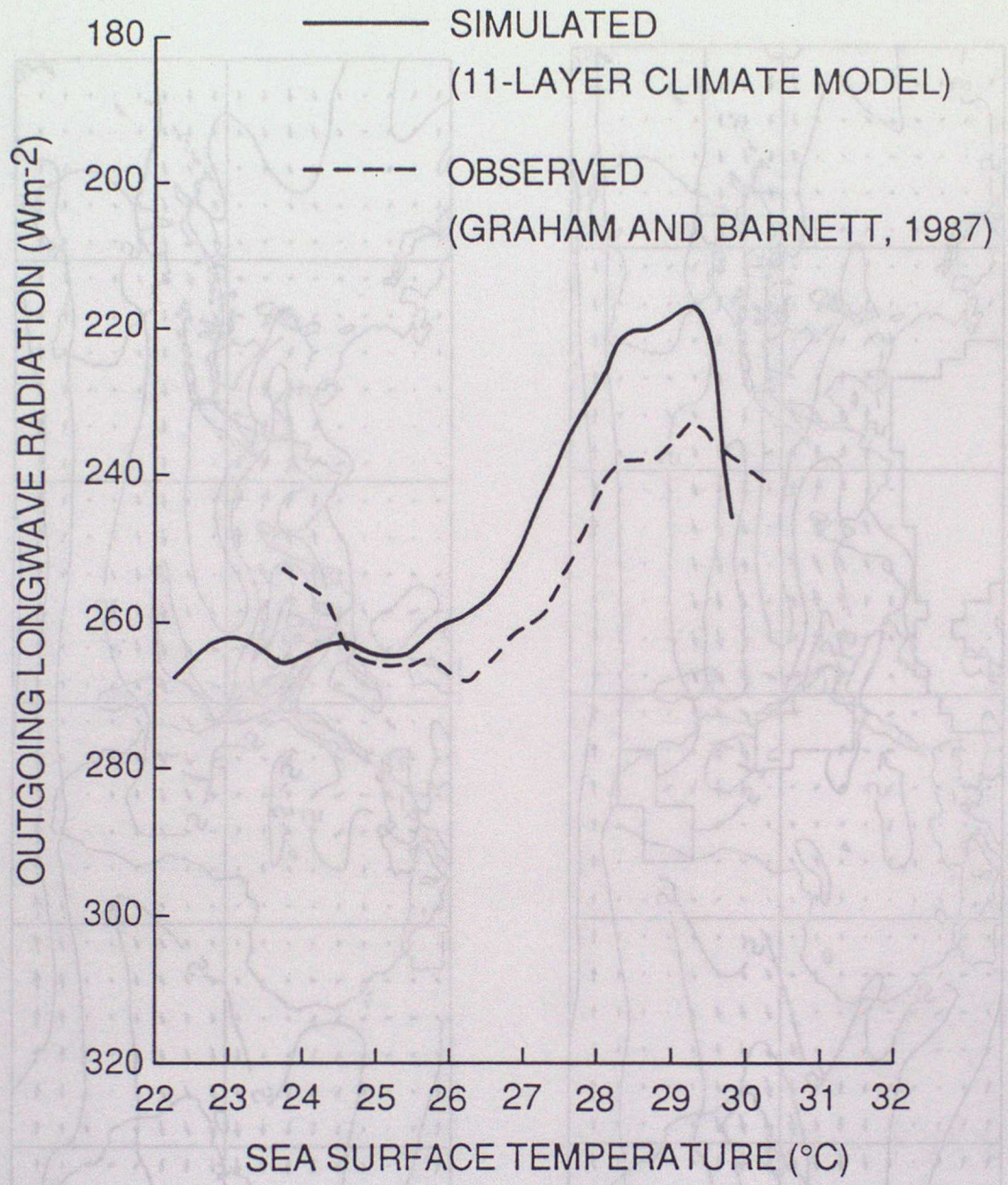

Figure 18. Plot of OLR against SST for convective grid points between 30°N and 30°S for a four year integration of an 11 - layer AGCM (———) compared with the results of an observational study (Graham and Barnett (1987)) (-----).

(a) SUMMER

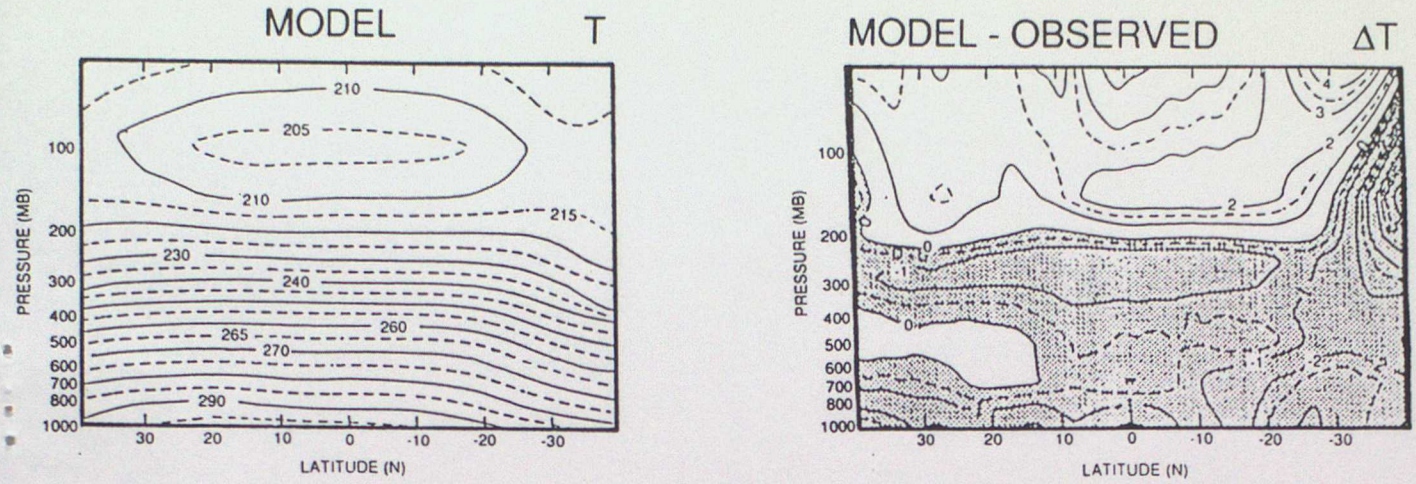

(b) WINTER

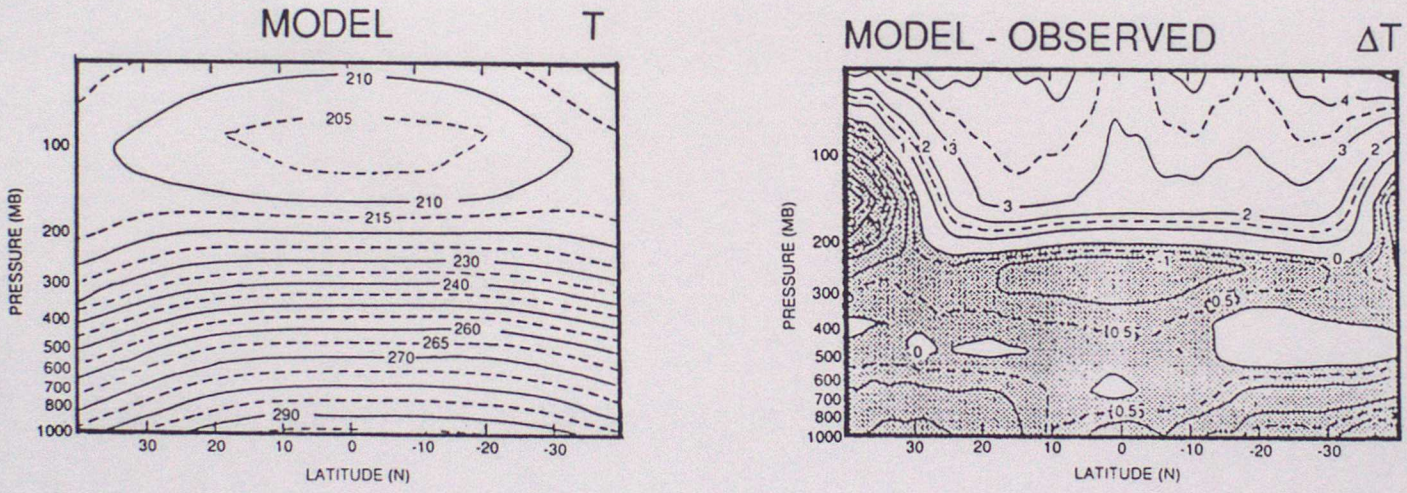

Figure 19. Height - latitude diagrams of zonal mean temperature for the tropics and sub-tropics of a four year integration of an 11 - layer AGCM and difference from an observed climatology (as fig. 16) for (a) Winter, (b) Summer.

DYNAMICAL CLIMATOLOGY TECHNICAL NOTES

DCTN 1	June 1984	A scheme for incorporating the thermodynamic sea-ice model into a coupled ocean-atmosphere model. C Gordon and M Bottomley
DCTN 2	Sept 1984	The parametrization of the upper ocean mixed layer in coupled ocean/atmosphere models. C Gordon and M Bottomley
DCTN 3	Sept 1984	The response of a simple thermodynamic sea-ice model to GCM forcing appropriate for perennial sea-ice. M Bottomley
DCTN 4	Sept 1984	Potential vorticity in the stratosphere derived using data from satellites. S A Clough, N S Grahame and A O'Neill
DCTN 5	Sept 1984	Simulation of the seasonal cycle of SST using globally specified climatological data to force simple ocean models. N S Grahame
DCTN 6	Sept 1984	Development of an improved GCM radiation scheme. A Slingo and R C Wilderspin
DCTN 7	Sept 1984	On the specification of surface fluxes in coupled atmosphere/ocean general circulation models. J F B Mitchell, C A Wilson and C M Price
DCTN 8	Sept 1984	A survey of possible repercussions of the Soviet river reversal programme on Arctic sea-ice. M Cattle
DCTN 9	Oct 1984	A study of a strong stratospheric warming during January 1982 T D A Fairlie
DCTN 10	Nov 1984	An intercomparison of the Met O 11 M45 model and the Met O 20 11-level model on the Cyber 205 J F Dyson
DCTN 11	Nov 1984	Simulation of observed time series of temperature and precipitation over eastern England. D M Reed
DCTN 12	Nov 1984	Forecasts and analyses of the onset of the Southwest monsoon. R Kershaw
DCTN 13	Nov 1984	On modelling the effects of CO_2 on climate. J F B Mitchell
DCTN 14	Dec 1984	Development of a revised longwave radiation scheme for an atmospheric general circulation model. A Slingo and R C Wilderspin
DCTN 15	Jan 1985	Rossby wavetrains in the stratosphere forced by localised disturbances in the troposphere. C J Marks (Oxford), A O'Neill and V D Pope

DYNAMICAL CLIMATOLOGY TECHNICAL NOTES

DCTN 16	Jan 1985	Observing system experiments using the Meteorological Office's 15-level model. M A Bromley
DCTN 17	Feb 1985	Atmospheric general circulation simulation of the climate of the Mediterranean region. M Cattle
DCTN 18	Feb 1985	Diurnal variation and cloud in a general circulation model. C A Wilson and J F B Mitchell
DCTN 19	Feb 1985	The sensitivity of the Saharan region in a general circulation model. W M Cunnington and P R Rowntree
DCTN 20	Mar 1985	The impact of aircraft observations on analyses and forecasts from the operational 15-level model. B R Barwell
DCTN 21	Mar 1985	Non-linear effects on heat-induced circulation of the tropical atmosphere. A E Gill and P J Phlips
DCTN 22	Apr 1985	Simulation of cloudiness with the U.K. Meteorological Office 11-layer AGCM. A Slingo and R C Wilderspin
DCTN 23	Apr 1985	An integrated approach to the representation of cloud processes. R N B Smith
DCTN 24	May 1985	Nuclear Winter: Calculations of the shortwave radiative effects of soot aerosols. A Slingo and P Goldsmith
DCTN 25	Jul 1985	Sea ice and the Antarctic winter circulation: a numerical experiment. J F B Mitchell and T S Hills
DCTN 26	Jul 1985	A Budyko-Sellers model for study of ocean-atmosphere interaction. W J Ingram
DCTN 27	Aug 1985	The effect of a shoaling thermocline on equatorially-trapped Kelvin waves. A E Gill and B A King
DCTN 28	Sept 1985	CO_2 climate sensitivity and model dependence of results. J F B Mitchell, C A Wilson and W M Cunnington
DCTN 29	Sept 1985	Handbook of the Meteorological Office 11-layer atmospheric general circulation model. Volume 1 : Model Description Edited by A Slingo
DCTN 30	Sept 1985	Impact of land surface variations on African rainfall in general circulation models. P R Rowntree, M F Wilson and A B Sangster

DYNAMICAL CLIMATOLOGY TECHNICAL NOTES

DCTN 31 Nov 1985 — The annual cycle of sea level in the eastern tropical Pacific.
G R Bigg and A E Gill

DCTN 32 Nov 1985 — An analytic model of the heat-induced tropical circulation in the presence of a mean wind.
P J Phlips and A E Gill

DCTN 33 Nov 1985 — The effect of resolution and diffusion on the simulated climate.
J F Dyson

DCTN 34 Jan 1986 — Rossby adjustment over a step.
M K Davey, A E Gill, E R Johnson and P F Linden

DCTN 35 Jan 1986 — Issues concerning the evaluation of effective surface roughness of heterogeneous terrain.
D J Carson

DCTN 36 Mar 1986 — Climate sensitivity and past climates : evidence from numerical studies
J F B Mitchell

DCTN 37 Mar 1986 — Parametrizations of land-surface processes in Meteorological Office numerical weather prediction and climate models
D J Carson

DCTN 38 Apr 1986 — Modelling of land-surface processes and their influence on European Climate
D A Warrilow, A B Sangster and A Slingo

DCTN 39 Apr 1986 — Simulation of climatic change due to increased CO_2
J F B Mitchell

DCTN 40 May 1986 — On the interpretation of the Eliassen-Palm flux divergence. Part I : Theory
D G Andrews

DCTN 41 June 1986 — Experiments on tropical circulation with a simple moist model.
M K Davey and A E Gill

DCTN 42 Jun 1986 — Parameter regimes for studying isolated eddies.
P D Killworth and M K Davey

DCTN 43 Jun 1986 — A comparison of the impact of an envelope orography and of a parametrization of orographic gravity-wave drag on model simulations.
A Slingo and D W Pearson

DCTN 44 Jul 1986 — The effect of a sea-surface temperature anomaly on a prediction of the onset of the south-west monsoon over India.
R Kershaw

DCTN 45 Jul 1986 — An introduction to the parametrization of land-surface processes.
D J Carson

DYNAMICAL CLIMATOLOGY TECHNICAL NOTES

DCTN 46 Sept 1986 — Lateral boundaries and the heat-induced flow in the tropical atmosphere.
P J Phlips and A E Gill

DCTN 47 Nov 1986 — Simulation of the diurnal cycle of outgoing longwave radiation with an atmospheric GCM.
A Slingo, R C Wilderspin and S J Brentnall

DCTN 48 Feb 1987 — A 2 x CO_2 climate sensitivity experiment with a global climate model including a simple ocean
C A Wilson and J F B Mitchell

DCTN 49 Feb 1987 — Sensitivity of the Met O 20 11-layer model to increased land surface roughness length
C C Heasman

DCTN 50 Feb 1987 — The influence of atmospheric waves on the general circulation of the middle atmosphere
D G Andrews

DCTN 51 Feb 1987 — Transport mechanisms in the middle atmosphere: an introductory survey
D G Andrews

DCTN 52 Mar 1987 — The Met O 20 stratosphere-mesosphere model
M Fisher

DCTN 53 Apr 1987 — Simulations of linear and nonlinear disturbances in the stratosphere
A O'Neill and V D Pope

DCTN 54 Apr 1987 — Aspects of dynamics of the middle atmosphere inferred using data from a satellite and from a numerical model
T D A Fairlie and A O'Neill

DCTN 55 Apr 1987 — The seasonal evolution of the stratosphere in the northern hemisphere
A O'Neill and V D Pope

DCTN 56 Apr 1987 — The adjustment of numerical weather prediction models to local perturbations
B R Barwell and R A Bromley

DCTN 57 Jun 1987 — Climate simulations for 9000 years before present: Seasonal variations and the effect of the Laurentide ice sheet
J F B Mitchell, N S Grahame and K J Needham

DCTN 58 Aug 1987 — Climatic effects of nuclear war: the role of atmospheric stability and ground heat fluxes.
J F B Mitchell and A Slingo

DCTN 59 Oct 1987 — The stratospheric major warming of winter 1984/85: observations and dynamical inferences.
T D A Fairlie and A O'Neill

DCTN 60 Oct 1987 — Some comparisons between the middle atmosphere dynamics of the southern and northern hemispheres
D G Andrews

	Jan 1988	Early winter in the northern stratosphere. M N Juckes and A O'Neill
DCTN 62	Feb 1988	Single column model tests of the Rowntree convection scheme using GATE data. D Gregory
DCTN 63	Mar 1988	The antarctic winter; simulations with climatological and reduced sea-ice extents. J F B Mitchell and C A Senior
DCTN 64	Mar 1988	An investigation of the Gates asynchronous coupling strategy using a simple energy-balance model. D L Roberts
DCTN 65	Apr 1988	The effect of improved physical parametrizations on simulations of cloudiness and the earth's radiation budget. A Slingo, R C Wilderspin and R N B Smith
DCTN 66	May 1988	Comparison of data and derived quantities for the middle atmosphere of the southern hemisphere. W L Grose and A O'Neill
DCTN 67	Aug 1988	Progress and future developments in modelling the climate system with general circulation models. P R Rowntree
DCTN 68	Aug 1988	A scheme for predicting layer clouds and their water content in a general circulation model. R N B Smith
DCTN 69	Nov 1988	Modelling climate change: an assessment of sea-ice and surface albedo feedbacks. W J Ingram, C A Wilson and J F B Mitchell
DCTN 70	Dec 1988	The "greenhouse" effect and climate change J F B Mitchell
DCTN 71	Dec 1988	On the dependence of climate sensitivity on convective parametrization. W M Cunnington and J F B Mitchell
DCTN 72	Dec 1988	Land surface parametrizations - basic concepts and review of schemes. P R Rowntree
DCTN 73	Jan 1989	Climate sensitivity: model dependence of results. J F B Mitchell
DCTN 74	Jan 1989	Parametrization of the upper ocean mixed layer in a tropical ocean GCM. S Ineson and C Gordon
DCTN 75	Mar 1989	A simple tropical coupled ocean-atmosphere model. C R Budin and M K Davey

DCTN 76	Jun 1989	The needs of general circulation models for runoff data. P R Rowntree
DCTN 77	Jul 1989	General circulation modelling of the atmosphere. J F B Mitchell
DCTN 78	Jul 1989	A model simulation of the seasonal cycle in the tropical Pacific Ocean using climatological and modelled surface forcing. C Gordon and R A Corry
DCTN 79	Jul 1989	Climatic impact of Amazon deforestation. J Lean and D A Warrilow
DCTN 80	Sept 1989	Surface evaporation during free convection. C Gordon and D L Hunt